Operational Certification Horizons in Quantum Transport: Copy Time, Conservation Laws, and a Rigorous Diffusive Benchmark

Sacha Mohamed *

Posted Date: 27 February 2026

doi: 10.20944/preprints202601.0364.v3

Keywords: quantum hypothesis testing; trace distance; information propagation; conservationlaws; diffusion; operator hydrodynamics; tensor networks

 doi:10.20944/preprints202601.0364.v3

Article

Operational Certification Horizons in Quantum Transport: Copy Time, Conservation Laws, and a Rigorous Diffusive Benchmark

Sacha Mohamed

Independent Researcher, Morocco; www.sachamed@gmail.com

Abstract

We introduce *quantum information copy time* as a task-defined latency for transport: it is the earliest time at which a receiver confined to a region B can certify, with prescribed advantage, which of two global hypotheses was prepared by local operations in a distant sender region A. The benchmark definition is information-theoretic—the Helstrom advantage on B, given by the trace distance between reduced states—and it admits natural refinements that incorporate explicit measurement restrictions (few-body and moment channels). We first derive kinematic locality constraints for Hamiltonian/Lindbladian dynamics with Lieb–Robinson tails and for circuits/quantum cellular automata with strict light cones. We then establish a theorem-level diffusive benchmark in the quantum symmetric simple exclusion process (Q-SSEP): for locally prepared charge-biased hypotheses, the *Helstrom* copy time obeys an unconditional diffusion-limited lower bound expressed in terms of the diffusion constant D and the static susceptibility χ. For closed Hamiltonian systems we formulate, with assumptions stated explicitly, a projection-based route that ties restricted copy times to a single slow transport pole on a diagnostically checkable time window. We provide conservative exact-diagonalization diagnostics in the XXZ chain together with a bundled TEBD/MPS reference implementation and convergence protocol (Supplementary S2 and Code SC1), validated against exact evolution on small sizes; large-L TEBD studies are left as future work. Finally, we contrast copy time with scrambling diagnostics based on out-of-time-ordered correlators and identify regimes in which conservation laws delay certifiability well beyond the ballistic operator-growth front.

Keywords: quantum hypothesis testing; trace distance; information propagation; conservation laws; diffusion; operator hydrodynamics; tensor networks

Introduction

Transport in quantum many-body systems is usually inferred from expectation values and correlation functions, while information-theoretic diagnostics are often framed in terms of operator growth and scrambling. This work takes a complementary, task-defined viewpoint. We ask when a localized perturbation prepared in a sender region A becomes *remotely certifiable* by an observer restricted to a distant region B. The resulting timescale—the *quantum information copy time*—is defined by binary hypothesis testing on B: it is the earliest time at which the receiver can distinguish two evolving global hypotheses with a prescribed advantage.

Two aspects make this perspective useful for transport theory. First, it cleanly separates *kinematics* from *mechanism*: locality bounds constrain when influence can begin, but they do not identify which dynamical sector controls a concrete certification task. Second, in systems with conservation laws the sector that dominates certifiability can be parametrically slower than the fastest operator-growth sector. In particular, ballistic growth of commutators (and large OTOCs) does not imply that a charge-biased hypothesis becomes certifiable at a comparable time; the bottleneck may be diffusive (or sub-/super-diffusive) transport of the conserved bias.

 doi:10.20944/preprints202601.0364.v3

A central aim of this manuscript is to put this statement on a precise footing without conflating ideal and experimentally accessible receivers. Accordingly, we distinguish two notions throughout: (i) the *Helstrom* copy time, defined by the trace distance between reduced states on B (equivalently, optimal measurements on B), and (ii) *restricted* copy times, where the receiver is constrained to a specified measurement/observable class (few-body, moment channels, coarse-grained charge, etc.). The restricted notion is the natural object when one wants scaling claims tied to hydrodynamic transport; the Helstrom notion is the mathematically canonical benchmark.

Main Contributions.

1. **Operational framework.** We define receiver advantage and copy time as a task-defined latency, and we provide a receiver-class refinement that makes measurement restrictions explicit (Section 2.1).
2. **Minimal locality constraints.** For Hamiltonian/Lindbladian dynamics with Lieb–Robinson tails and for circuits/QCAs with strict light cones, we derive a kinematic lower bound on copy time that isolates the threshold dependence and constants (Section 3).
3. **A rigorous diffusive benchmark (Q-SSEP).** In a controlled, locality-preserving diffusive model—the quantum symmetric simple exclusion process (Q-SSEP)—we prove an *unconditional* lower bound of the form

$$\tau_{\mathrm{copy}}(A \to B; \eta) \;\geq\; C(\eta, \epsilon, \chi, |A|, |B|)\, \frac{\ell^2}{D},$$

where $\ell = d(A, B)$, D is the diffusion constant of the conserved density, and χ is the associated static susceptibility. This provides a theorem-level instance in which diffusion-limited *Helstrom* copying can be established without any fast-mixing closure (Section 6; Supplementary S3).

4. **Hydrodynamic translation for unitary systems (conditional but testable).** For closed Hamiltonian dynamics we formulate a projection-based route from charge bias to receiver advantage and identify the concrete hypotheses required for a single-mode window (Sections 4–5). We treat the closure assumptions explicitly as assumptions rather than as universal theorems.
5. **Benchmarking and protocols.** we provide conservative finite-size transport diagnostics in the XXZ chain and a detailed TEBD/MPS protocol outline with a convergence checklist (Section 10; Supplementary S2). We emphasize that no main-text scaling claim relies on TEBD results or TEBD-specific code.
6. **Comparison to scrambling diagnostics and extensions.** We confront copy time with OTOCs and explain, at the level of a sharp separation, why a ballistic OTOC front can coexist with diffusion-limited certifiability under conservation laws (Section 8). We also outline how copy time can act as an operational microscope for non-diffusive regimes (KPZ superdiffusion, Griffiths subdiffusion, MBL) (Supplementary S4).

Positioning.

Receiver advantage is the trace distance between reduced states and is standard in quantum hypothesis testing [1,2]. What is emphasized here is the *hitting-time* interpretation at fixed advantage and, crucially, the way conservation laws and receiver restrictions can turn transport coefficients into operational latencies. This connects naturally to the linear-response and projection-operator traditions [3–6] and to recent work on operator hydrodynamics in conserving dynamics [7,8]. The diffusive benchmark (Q-SSEP) provides a controlled setting in which the operational inequality becomes fully rigorous, while the unitary sections describe how and when similar bounds should emerge in Hamiltonian systems.

Operational Definition and Preliminaries

 doi:10.20944/preprints202601.0364.v3

Copy Time as Receiver-Limited Hypothesis Testing

Fix disjoint lattice regions A (sender) and B (receiver). To avoid ambiguity about "support in A", we take the hypotheses to be prepared from a common reference state ρ_{ref} by *local* channels on A:

$$\rho_{\pm}(0) = \Lambda_A^{\pm}(\rho_{\mathrm{ref}}), \qquad \Lambda_A^{\pm} = \Lambda_A^{\pm} \otimes \mathrm{id}_{A^c}.$$

This guarantees $\rho_+(0)$ and $\rho_-(0)$ coincide on A^c. The evolved hypotheses are $\rho_{\pm}(t) = \mathcal{U}_t\left(\rho_{\pm}(0)\right)$, where $\mathcal{U}_t$ is a unitary channel (closed dynamics) or, more generally, any CPTP dynamics. For the receiver region B, let $\rho_{\pm,B}(t) = \mathrm{Tr}_{B^c}\rho_{\pm}(t)$.

Definition 1 (Receiver advantage and copy times). *[1,2] Fix a threshold* $\eta \in (0,1)$.

1. **Helstrom (unrestricted) advantage.** The optimal receiver advantage is

$$\mathrm{Adv}_{A\to B}^{\mathrm{full}}(t) := \frac{1}{2}\left\|\rho_{+,B}(t) - \rho_{-,B}(t)\right\|_1,$$

equivalently the Helstrom bias for discriminating $\rho_{+,B}(t)$ vs. $\rho_{-,B}(t)$ with equal priors. The associated copy time is

$$\tau_{\mathrm{copy}}^{\mathrm{full}}(A \to B; \eta) := \inf\{t \geq 0 : \mathrm{Adv}_{A\to B}^{\mathrm{full}}(t) \geq \eta\}.$$

2. **Restricted advantage.** Let $\mathcal{O}_B$ be an admissible observable class on B with $\| O_B \|_\infty \leq 1$ for all $O_B \in \mathcal{O}_B$ (few-body algebras, moment channels, coarse-grained charge observables, etc.). Define the restricted advantage

$$\mathrm{Adv}_{A\to B}^{\mathcal{O}}(t) := \frac{1}{2}\sup_{O_B \in \mathcal{O}_B} \mathrm{Tr}\left[O_B(\rho_{+,B}(t) - \rho_{-,B}(t))\right],$$

and the corresponding restricted copy time $\tau_{\mathrm{copy}}^{\mathcal{O}}(A \to B; \eta) := \inf\{t \geq 0 : \mathrm{Adv}_{A\to B}^{\mathcal{O}}(t) \geq \eta\}$ by the same hitting-time rule as in [eq:copytime]. Equivalently, if $\Phi_{\mathcal{O}}$ denotes a CPTP "measurement compression" channel whose dual maps the unit ball into $\mathcal{O}_B$, then $\mathrm{Adv}^{\mathcal{O}}(t) = \frac{1}{2}\| \Phi_{\mathcal{O}}\left(\rho_{+,B}(t) - \rho_{-,B}(t)\right) \|_1$.

By data processing, $\mathrm{Adv}_{A\to B}^{\mathcal{O}}(t) \leq \mathrm{Adv}_{A\to B}^{\mathrm{full}}(t)$ and hence $\tau_{\mathrm{copy}}^{\mathrm{full}}(A \to B; \eta) \leq \tau_{\mathrm{copy}}^{\mathcal{O}}(A \to B; \eta)$. Most transport-driven scaling statements in this manuscript concern *restricted* copy times, because conservation laws naturally constrain the evolution of coarse observables. The rigorous diffusive benchmark in Section 6 applies to the *Helstrom* copy time.

Operational Sampling Complexity (How Many Shots?).

"Operational" is meaningful only if the advantage can be estimated with a controlled number of experimental samples. For a fixed time t and an observable O_B with eigenvalues in $[-1,1]$, an empirical estimator $\widehat{m} = \frac{1}{n}\sum_{j=1}^{n} o_j$ of $m = \mathrm{Tr}\left(O_B\, \delta\rho_B(t)\right)$ obeys a Hoeffding bound: $n = \Theta(\delta^{-2}\log(1/\alpha))$ samples suffice to estimate m to additive error δ with failure probability α. Consequently, certifying $\mathrm{Adv}_{A\to B}^{\mathcal{O}}(t) \geq \eta$ up to slack δ requires $n = O\left(\delta^{-2}\log(1/\alpha)\right)$ shots for each candidate O_B (or for the compressed measurement channel $\Phi_{\mathcal{O}}$). For the special case $B =$ one site and charge-biased hypotheses (Section 10.2), the Helstrom-optimal measurement is a single

 doi:10.20944/preprints202601.0364.v3

local two-outcome measurement, so the same $O(\delta^{-2}\log(1/\alpha))$ scaling applies without tomography.

Remark on "Chemical Potential Tilts".

Later we use the convenient parametrization $\rho_{\pm}(0) \propto e^{-\beta H \mp \epsilon Q_A}$ in linear-response calculations. At finite β this family is not strictly supported in A unless $[H, Q_A] = 0$; it should be regarded as an analytically tractable proxy for a locally prepared bias, with errors controlled by equilibrium clustering. Whenever strict support in A is required (for locality-limited bounds), we work with the local-channel preparation [eq:local_prep].

Elementary Bounds and Caveats

We record two standard inequalities used later. The first is a direct duality bound.

Lemma 1 (Standard tool: trace-norm duality). *This identity is standard in quantum hypothesis testing and is included only to fix notation. For any Hermitian* X *and any observable* O *with* $\| O \|_\infty \leq 1$, $|\mathrm{Tr}(OX)| \leq \| X \|_1$. *In particular,* $\mathrm{Adv}^{\mathrm{full}}_{A\to B}(t) = \frac{1}{2} \sup_{\|O_B\|_\infty \leq 1} \mathrm{Tr}\big[O_B(\rho_{+,B}(t) - \rho_{-,B}(t))\big]$.

The second is Pinsker's inequality. We state the required support condition explicitly.

Lemma 2 (Pinsker inequality with full-rank condition). *If* ρ *is full rank (so that* $D(\sigma \| \rho) < \infty$ *for all* σ*), then* $D_{\mathrm{tr}}(\sigma, \rho) \leq \sqrt{\frac{1}{2} D(\sigma \| \rho)}$. *If* ρ *is not full rank, the inequality remains valid provided* $\mathrm{supp}(\sigma) \subseteq \mathrm{supp}(\rho)$*; otherwise* $D(\sigma \| \rho) = \infty$ *and [eq:pinsker] is vacuous.*

In all numerical benchmarks reported below we work in finite-dimensional Hilbert spaces (finite spin chains) and, where thermal reference states are invoked, at finite inverse temperature $\beta < \infty$; consequently the reduced density matrices encountered are effectively full rank (up to machine precision), and Lemma 2 is used only in this non-vacuous regime.

Minimal Locality Bounds and What Is Genuinely Nontrivial

Locality-Preserving Dynamics and Lieb–Robinson Constraints

Throughout, we assume a lattice with a metric $d(\cdot,\cdot)$, and we denote the distance between regions A, B by $d(A, B)$. For continuous-time local Hamiltonians or for locality-preserving circuits/QCAs, the standard consequence is a Lieb–Robinson-type bound: a local perturbation cannot influence distant observables faster than a finite velocity v_{LR}, up to exponentially small tails.

We deliberately *do not* conflate different settings. When we refer to LR bounds, we mean either (i) a continuous-time Hamiltonian/Lindbladian LR bound with constants (v, μ) or (ii) a circuit/QCA strict light cone. In each case, the structure is an upper bound on commutators of evolved local observables.

Theorem 3 (Locality-limited copying: Hamiltonian LR tails vs. circuit/QCA light cones). *Let* $\mathcal{U}_t$ *be the evolution channel (unitary or CPTP) on a lattice with metric* $d(\cdot,\cdot)$*. Assume one of the following standard locality structures for Heisenberg-evolved observables.*

(H) Continuous-time Hamiltonian/Lindbladian (Lieb–Robinson tails). *There exist constants* $c, \mu, v > 0$ *such that for any observables* O_X *supported on a finite region* X *and* O_Y *supported on* Y, $\| [O_X(t), O_Y] \|_\infty \leq c\,|X|\,|Y|\,\| O_X \|_\infty \| O_Y \|_\infty\, e^{-\mu\,(d(X,Y) - v|t|)}$.

 doi:10.20944/preprints202601.0364.v3

(C) Discrete-time range-R circuits / reversible QCAs (strict light cone). *For each integer time* $t \in \mathbb{N}$*, the Heisenberg image of a local algebra satisfies* $\mathrm{supp}(O_X(t)) \subseteq X^{+Rt} \quad \Rightarrow \quad [O_X(t), O_Y] = 0$ whenever $d(X,Y) > Rt$.

Let the initial pair $\rho_\pm$ *differ only inside a sender region* A *and satisfy* $\| \rho_+ - \rho_- \|_1 \leq 2$*. Then for any receiver region* B *and any time* t*:*

- *(H) For local Hamiltonian evolution satisfying a Lieb–Robinson bound, the receiver advantage is bounded by [eq:lr_finish] outside the effective cone.*
- *(C) For range-R circuits or reversible QCAs, the strict light cone implies* $Adv^{full}_{A\to B}(t) = 0$ *whenever* $d(A,B) > Rt$*.*

In particular, in both settings the copy time obeys the kinematic lower bound $\tau^{\mathrm{full}}_{\mathrm{copy}}(A \to B; \eta) \geq \begin{cases} \frac{d(A,B)}{v} - \frac{1}{\mu v}\log(C_{\mathrm{LR}}/\eta), & \text{in (H)}, \\ d(A,B)/R, & \text{in (C)}. \end{cases}$

Remark 4 (About constants in the Lieb–Robinson bound). *In case (H), one may take* $C_{\mathrm{LR}} := 2c\,|A|\,|B|\,\| \rho_+ - \rho_- \|_1$ *for the LR prefactor* c *appearing in [eq:lr_localization] (up to harmless constants absorbed by the choice of norm convention), so that the only dependence on* A, B *is through the region-size factor* $|A||B|$*. If the initial preparation is not strictly supported in* A *but has exponential Gibbs tails with rate* κ (i.e. $\| \mathrm{Tr}_{A^c}\delta\rho \|_1$ *decays as* $e^{-\kappa\, d}$*), the same bound holds with an additional additive error term of order* $e^{-\kappa(d(A,B)-v|t|)}$*; equivalently one replaces* μ *by* $\min\{\mu, \kappa\}$ *in the logarithmic correction. In case (H), the prefactor* C_{LR} *comes from the standard LR "localization" estimate [eq:lr_localization] (denoted* C_1 *in the proof) and is independent of* A, B, t *except through bounded region-size factors. The only scaling content of [eq:lr_tau_lower] is therefore the kinematic term* $d(A,B)/v$ *and the mild logarithmic threshold correction.*

Remark 5 (What Theorem 3 *does not do).* *Theorem 3 is an upper bound on how early copy can occur; it does not provide a mechanism for achieving* η *at times* $t \sim d(A,B)/v$*. For an A-level contribution, the hard part is a lower bound (or matching scaling) in physically relevant regimes. This is precisely where conservation laws and hydrodynamics enter.*

Conservation Laws and an Explicit Receiver Class

Fix a (quasi-)local conserved charge $Q = \sum_x q_x$ with $[\mathcal{U}_t, Q] = 0$. We will focus on initial perturbations that are "charge-biased" in A. Importantly, the receiver need not have access to all observables on B; in realistic settings one often restricts to a class $\mathcal{O}_B$ (e.g., low moments of charge, or few-body observables).

To avoid circularity, we proceed in two steps: (i) we provide a theorem under *minimal* hypotheses that yields a general lower bound in terms of an explicitly defined susceptibility-like object, and (ii) we identify an additional *single-mode hydrodynamic window* under which that object becomes computable from transport data.

Hydrodynamic Closure: from Charge Bias to Spectral Susceptibility

Notation Used in the Hydrodynamic Closure Section.

Symbol	Meaning
$\mathscr{L}$	Liouvillian superoperator ($\mathscr{L}(O) = i[H, O]$ for closed systems)
$\mathcal{P}$, $\mathcal{Q}$	Mori projection onto the slow manifold and its complement
$\langle\cdot,\cdot\rangle_\beta$	Kubo–Mori inner product induced by the reference state ρ_β
$\mathscr{L}_{\mathrm{eff}}$	Markovianized effective slow-sector generator (Eq. [eq:Leff])
$\chi^{(2)}_{A\to B}$	Second-moment spectral susceptibility (Definition 2)
J_B	Receiver observable restricted to the slow sector

 doi:10.20944/preprints202601.0364.v3

Δ_{fast} Fast-sector mixing gap controlling memory decay (assumption)

Setup: Local Equilibrium Manifold and Linearization

Let ρ_β be a reference Gibbs (or generalized Gibbs) state at inverse temperature β. Consider a small sender perturbation of "chemical potential" type,

$$\rho_\pm(0) = \frac{e^{-\beta H \mp \epsilon Q_A}}{\mathrm{Tr}(e^{-\beta H \mp \epsilon Q_A})},$$

where $Q_A = \sum_{x\in A} q_x$ and $\epsilon \ll 1$. To leading order in ϵ, the difference $\delta\rho(0) := \rho_+(0) - \rho_-(0)$ is linear in Q_A in the Kubo–Mori inner product.

A Principled Definition of the Second-Moment Susceptibility

Let $\mathscr{L}$ denote the (Heisenberg) Liouvillian superoperator $\mathcal{L}(O) = i[H, O]$ (or the generator of a CPTP semigroup in open settings). Let $\mathcal{P}$ be a projection onto the slow subspace spanned by the conserved density modes; concretely, $\mathcal{P}$ is the Mori projection with respect to the Kubo–Mori inner product. Define the reduced (effective) slow-sector operator using the Mori–Zwanzig projection formalism [4,5]. In Laplace space one obtains an exact identity for the projected dynamics,

$$(z - \mathcal{L}_{\text{eff}}(z))^{-1} \;=\; \mathcal{P}\,(z - \mathcal{L})^{-1}\,\mathcal{P}, \qquad \mathcal{L}_{\text{eff}}(z) := \mathcal{P}\mathcal{L}\mathcal{P} \;+\; \mathcal{P}\mathcal{L}\mathcal{Q}\,(z - \mathcal{Q}\mathcal{L}\mathcal{Q})^{-1}\,\mathcal{Q}\mathcal{L}\mathcal{P}.$$

This expression is exact but generally nonlocal in time (the z-dependence encodes a memory kernel). In *closed unitary* dynamics, $\mathcal{L}(O) = i[H, O]$ is anti-self-adjoint and $\mathcal{L}_{\text{eff}}(z)$ is *not* a CPTP generator in general; it should be interpreted as a reduced linear-response operator in the Kubo–Mori geometry. In contrast, for genuinely open Markovian dynamics (Lindbladians) the same construction yields a bona fide dissipative generator on the slow manifold.

To obtain a usable closure we adopt a standard *Markovianized* approximation on a time window where the fast sector mixes rapidly: we replace $\mathcal{L}_{\text{eff}}(z)$ by its low-frequency limit $\mathcal{L}_{\text{eff}} := \mathcal{L}_{\text{eff}}(0)$ and assume that the fast subspace $\mathcal{Q}$ has a spectral gap $\Delta_{\text{fast}} > 0$ that controls memory decay. Under these hypotheses one recovers the familiar time-local approximation

$$\mathcal{L}_{\text{eff}} \approx \mathcal{P}\mathcal{L}\mathcal{P} \;-\; \mathcal{P}\mathcal{L}\mathcal{Q}\,(\mathcal{Q}\mathcal{L}\mathcal{Q})^{-1}\,\mathcal{Q}\mathcal{L}\mathcal{P},$$

which we use in the theorems below, with an explicit error term quantifying the leakage into $\mathcal{Q}$ (see Proposition 7 and Theorem 8).

Assumptions and Expected Domain of Validity.

The Markovianized Mori closure is a *conditional* statement: it is expected to hold most cleanly in chaotic, finite-temperature phases with a *clear separation* between a small set of conserved slow modes and a rapidly mixing fast sector. It can fail or require modification in integrable or near-integrable regimes, in many-body localized phases, when multiple slow modes with comparable rates coexist (or when long-time tails are important), and in settings with quasi-conservation that produces parametrically long prethermal plateaus. Accordingly, Theorem 10 and the scaling discussion below should be read as a *controlled closure under explicit diagnostics* (single-mode window, nonvanishing receiver overlap, and a fast-sector gap), not as an unconditional claim about generic dynamics.

Hydrodynamic closure assumptions (what is assumed, what can be checked, and typical failure modes). The single-mode statement in this section is intended to be applied only when the assumptions listed in the left column are plausibly satisfied.

Assumption	Operational/diagnostic proxy	Typical failure modes

 doi:10.20944/preprints202601.0364.v3

Fast-sector mixing ("gap" in $\mathcal{Q}$)	Rapid decay of generic local autocorrelations to their hydrodynamic tail; absence of long-lived nonconserved operators in the accessible ED window (finite-size diagnostic) (Supplementary diagnostics)	Integrability, quasi-conservation (prethermal plateaus), MBL
Single isolated slow pole	$\Gamma(k)$ approximately linear in k^2 over a time window; window-to-window stability; no competing ballistic/Drude channel (Sec. 9, Supplementary S2)	Multiple slow modes, long-time tails, Drude weight/nonzero stiffness
Nonzero receiver overlap	Choose J_B with provable overlap (e.g., coarse-grained charge in B); verify signal is nonzero at accessible times	Symmetry mismatch; receiver observable orthogonal to slow mode
Linear-response regime	Small ϵ tilt; check odd-in-ϵ scaling and absence of saturation artifacts in numerics	Large perturbations, finite-size saturation, edge effects

Definition 2 (Second-moment spectral susceptibility). *[3]–[5] Let $\delta\mu$ be a small chemical-potential profile supported in A, and let J_B denote a receiver observable* (e.g., *the charge in B or its low moments) projected to the slow subspace. We define the second-moment spectral susceptibility by*

$$\chi^{(2)}_{A\to B} := \langle J_B,\ (-\mathcal{L}_{\text{eff}})^{-2} J_B\rangle_\beta \ \|\ \delta\mu\ \|^2,$$

where $\langle\cdot,\cdot\rangle_\beta$ is the Kubo–Mori inner product and $(-\mathcal{L}_{\text{eff}})^{-2}$ is understood on the orthogonal complement of the zero mode.

Remark 6 (Why [eq:*chi2] is the right object). The operator $(-\mathcal{L}_{\text{eff}})^{-1}$ is a resolvent that weights modes by inverse decay rate; squaring it yields a second moment that controls the time at which a receiver observable can accumulate a finite signal. Definition 2 makes explicit (a) the operator being inverted, (b) the topology (Kubo–Mori norm) in which neglected modes are controlled, and (c) the receiver class through J_B.*

Proposition 7 (Fast-sector leakage bound in the Kubo–Mori topology). *Let $\langle\cdot,\cdot\rangle_\beta$ be the Kubo–Mori inner product induced by a full-rank reference state ρ_β, $\langle X,Y\rangle_\beta := \int_0^1 \mathrm{Tr}\,(\rho_\beta^s X^\dagger \rho_\beta^{1-s} Y)\,ds$, $\|X\|_\beta := \sqrt{\langle X,X\rangle_\beta}$. Assume that the fast-sector generator has a spectral gap $\Delta_{\text{fast}} > 0$ in this topology, in the sense that for all X with $\mathcal{P}X = 0$, $\langle X, -\mathcal{Q}\mathcal{L}\mathcal{Q}\,X\rangle_\beta \geq \Delta_{\text{fast}}\ \|X\|_\beta^2$. Then the leakage of slow data into the fast sector is exponentially suppressed: $\|\mathcal{Q}e^{t\mathcal{L}}\mathcal{P}\|_{\beta\to\beta} \leq e^{-\Delta_{\text{fast}}t}$. Consequently, for any receiver observable O_B with $\|O_B\|_\infty \leq 1$ and any slow-sector signal $X \in \mathrm{Ran}(\mathcal{P})$, $|\langle O_B,\ \mathcal{Q}e^{t\mathcal{L}}X\rangle_\beta| \leq \|O_B\|_\beta \|\mathcal{Q}e^{t\mathcal{L}}\mathcal{P}\|_{\beta\to\beta}\|X\|_\beta \leq \|O_B\|_\beta \|X\|_\beta\ e^{-\Delta_{\text{fast}}t}$. This provides an explicit (conservative) topology-controlled bound on the neglected-mode contribution in Theorem 8.*

Two Theorems: Minimal and Single-Mode

We now state two versions of the central result: a minimal statement and a single-mode hydrodynamic specialization.

Proposition 8 (Projection-operator bound on receiver advantage (conditional; explicit error term)). *Assume (i) a finite-dimensional lattice system with a full-rank reference state ρ_β, (ii) a weak charge-biased perturbation of the form [eq:tilt] with $\epsilon \ll 1$, and (iii) a Mori projection $\mathcal{P}$ onto the slow manifold such that the Markovianized effective operator $\mathcal{L}_{\text{eff}}$ in [eq:Leff] is well-defined on $\mathrm{Ran}(\mathcal{P})$. Let $J_B \in \mathrm{Ran}(\mathcal{P})$ be a receiver observable supported in B with $\|J_B\|_\infty \leq 1$. Then, for all times $t \geq 0$, $\mathrm{Adv}^{\mathcal{O}}_{A\to B}(t) \geq \frac{\epsilon}{2}|\langle J_B,\ e^{t\mathcal{L}_{\text{eff}}}\mathcal{P}(Q_A)\rangle_\beta| - \frac{\epsilon}{2}|\langle J_B,\ \mathcal{Q}e^{t\mathcal{L}}\mathcal{P}(Q_A)\rangle_\beta| + O(\epsilon^3)$. If, in addition, the fast-sector gap*

 doi:10.20944/preprints202601.0364.v3

hypothesis [eq:fast_gap] of Proposition 7 holds with rate Δ_{fast}*, then the neglected-mode term admits the explicit conservative bound* $|\langle J_B, \mathcal{Q}e^{t\mathcal{L}}\mathcal{P}(Q_A)\rangle_\beta| \leq \| J_B \|_\beta \| \mathcal{P}(Q_A) \|_\beta \; e^{-\Delta_{\mathrm{fast}}t}$*. Thus, on any time window where* $e^{-\Delta_{\mathrm{fast}}t} \ll 1$*, the receiver advantage is governed (up to explicit exponentially small leakage) by the projected slow dynamics, without assuming a priori that the receiver "sees the slow mode".*

Corollary 9 (Explicit "slow signal minus fast leakage" form). *Under the assumptions of Theorem 8 and Proposition 7, define* $S_{A\to B}(t) := |\langle J_B, e^{t\mathcal{L}_{\mathrm{eff}}}\mathcal{P}(Q_A)\rangle_\beta|, \qquad C_{\mathrm{fast}} := \| J_B \|_\beta \| \mathcal{P}(Q_A) \|_\beta$*. Then, for all* $t \geq 0$*,* $\mathrm{Adv}^{\mathcal{O}}_{A\to B}(t) \geq \frac{\epsilon}{2} S_{A\to B}(t) - \frac{\epsilon}{2} C_{\mathrm{fast}} e^{-\Delta_{\mathrm{fast}}t} + O(\epsilon^3)$*. In particular, once* $t \gg \Delta_{\mathrm{fast}}^{-1}$*, the advantage is controlled by the explicit slow-sector correlator* $S_{A\to B}(t)$ *up to a quantified error.*

Conditional Theorem 10 (Single-mode hydrodynamic window (conditional; checkable hypotheses)). *Assume the hypotheses of Theorem 8 together with:*

1. ***Single slow pole:*** *on a wavelength band* $k \in [k_{min}, k_{max}]$ *the slow spectrum on* $Ran(\mathcal{P})$ *consists of a single nonzero mode with decay rate* $\Gamma(k) = Dk^2 + o(k^2)$ *and a gap* Δ_2 *to the next slow mode on that band;*
2. ***Receiver overlap:*** *the projected receiver observable has nonzero overlap with that mode, quantified by the form factor* $F_B(k)$ *entering [eq:signal_k];*
3. ***Fast mixing:*** *the fast-sector leakage is controlled by Proposition 7 with rate* Δ_{fast} *on the window of interest.*

Then, for a one-dimensional sender–receiver separation $\ell = d(A,B)$ *and fixed threshold* $\eta \in (0,1)$*, the copy time satisfies the transport-limited scaling $$\label{eq:tau_scaling} \tau_{\mathrm{copy}}^{\mathcal{O}}(A\to B;\eta)=\frac{\ell^2}{4D}\Bigl(1+o(1)\Bigr)+O\!\bigl(t_0\,\log(C/\eta)\bigr),$$ where* $t_0 := 1/(Dk_{\mathrm{max}}^2)$ *is the microscopic time associated with the upper cutoff* k_{max} *of the single-mode window and* $C > 0$ *collects order-one receiver/form-factor constants (explicit in Appendix 14). In the hydrodynamic window* $\Delta_{\mathrm{fast}}^{-1} \ll t \ll \min\{L^2/D, \Delta_2^{-1}\}$*, with explicitly bounded systematic errors from: (i) finite-size discretization of* k *(Appendix 17), (ii) slow-sector multi-mode contamination* $O(e^{-\Delta_2 t})$*, and (iii) fast-sector leakage* $O(e^{-\Delta_{\mathrm{fast}}t})$ via *[eq:adv_error_explicit]. The prefactor can be expressed in terms of the susceptibility* $\chi^{(2)}_{A\to B}$ *in Definition 2.*

A full proof is given in Appendices 13–14. The key point is that the nontrivial input is *not* the statement "the receiver sees the slow mode"; rather it is the explicit control of $\mathcal{E}(t)$ and the explicit coupling coefficient between Q_A and J_B in the projected dynamics.

Worked Hydrodynamic Example: One-Dimensional Diffusion Kernel

To make Theorem 10 concrete, we work out the diffusion-kernel signal at the level needed to turn "diffusion implies $\tau \sim \ell^2$" into a quantitatively checkable statement.

Linear-Response Form of the Reduced-State Difference

Write $\rho_\pm(t) = \mathcal{U}_t\left(\rho_\pm(0)\right)$ with $\rho_\pm(0)$ given by [eq:tilt]. Expanding to first order in ϵ yields

$$\delta\rho(t) := \rho_+(t) - \rho_-(t) = \epsilon\, \mathcal{U}_t\big(\delta\rho_{Q_A}\big) + O(\epsilon^3),$$

where $\delta\rho_{Q_A}$ is the Kubo–Mori tangent vector associated to Q_A at ρ_β. For any receiver observable O_B with $\| O_B \|_\infty \leq 1$,

$$\mathrm{Tr}\big(O_B\, \delta\rho_B(t)\big) = \mathrm{Tr}\big(O_B\, \mathrm{Tr}_{B^c}\delta\rho(t)\big) = \mathrm{Tr}\big(O_B(t)\, \delta\rho_{Q_A}\big) + O(\epsilon^3).$$

 doi:10.20944/preprints202601.0364.v3

Thus the operational advantage is lower-bounded by any explicit choice of O_B.

Diffusion Equation for the Conserved Density

Assume a single conserved density $q(x)$ on a ring of length L with hydrodynamic equation

$$\partial_t\, \delta q(x,t) = D\ \partial_x^2\, \delta q(x,t),$$

valid on the window $t \in [t_0, t_1]$ and wavelengths $\lambda \gg 1$ (in lattice units). On the ring, the Fourier modes $k_n = \frac{2\pi n}{L}$ evolve as

$$\delta q_{k_n}(t) = e^{-Dk_n^2 t}\, \delta q_{k_n}(0).$$

For a localized initial bias in A, $\delta q(x,0)$ has broad Fourier support but its long-time profile is controlled by the smallest nonzero $|k_n|$.

Receiver Signal and a Concrete Threshold-to-Time Relation

Let $Q_B(t) = \int_B q\,(x,t)\,dx$ be the receiver charge in an interval B centered at distance ℓ from A with width w. In the linear-response regime around ρ_β, the expected receiver shift is proportional to the chemical potential profile with coefficient given by the static susceptibility $\chi = \partial\langle q\rangle/\,\partial\mu$:

$$\delta\langle Q_B(t)\rangle \approx \chi \int_B \delta\,\mu(x,t)\,dx.$$

Approximating $\delta\mu$ by the Gaussian heat kernel on $\mathbb{R}$ for times $t \ll L^2/D$,

$$\delta\mu(x,t) \approx \frac{\epsilon}{\sqrt{4\pi D t}} \exp\left(-\frac{(x-\ell)^2}{4Dt}\right),$$

we obtain the scaling

$$\delta\langle Q_B(t)\rangle \sim \epsilon\,\chi\, w\,(4\pi D t)^{-1/2} \exp\left(-\frac{\ell^2}{4Dt}\right),$$

up to relative corrections of order $w^2/(Dt)$ and tD/L^2. Choosing O_B proportional to the centered receiver charge (normalized to $\| O_B \|_\infty \leq 1$) and using Lemma 1 gives a lower bound

$$\mathrm{Adv}^{\mathrm{full}}_{A\to B}(t) \ \geq\ \frac{1}{2}\left|\mathrm{Tr}\big(O_B\,\delta\rho_B(t)\big)\right| \ \gtrsim\ c_0\,|\delta\langle Q_B(t)\rangle|,$$

where c_0 is an explicit normalization constant. Solving $\mathrm{Adv}^{\mathrm{full}}_{A\to B}(t) = \eta$ for t yields, at leading order,

$$\tau_{\mathrm{copy}}(A\to B;\eta) \approx \frac{\ell^2}{4D}\left[1 + O\left(\frac{\log(1/\eta)}{\log(\ell)}\right)\right],$$

making precise the statement that the *distance dependence* is ℓ^2 while η enters only logarithmically in the diffusive window.

A Quantitative η– and $|B|$–Dependence (Gaussian-Kernel Inversion).

Within the Gaussian-kernel approximation [eq:signal_scaling] (and keeping only the dominant ℓ-dependence), the threshold condition has the form

 doi:10.20944/preprints202601.0364.v3

$$K_B\, t^{-1/2}\exp\left(-\frac{\ell^2}{4Dt}\right) = \eta_{\text{eff}},$$

where $K_B \propto |\epsilon|\,\chi\,|B|$ collects receiver-dependent prefactors and η_{eff} is the effective threshold after mapping a chosen measurement to an advantage surrogate (e.g., in the commuting Gaussian model below, $\eta_{\text{eff}} \propto \text{erf}^{-1}(\eta)$). Equation [eq:threshold_kernel_form] can be inverted in closed form using the Lambert-W function:

$$\tau_{\text{copy}}(A \to B;\eta) \;\approx\; \frac{\ell^2}{2D}\,[-W_{-1}(-c\,\frac{\ell^2\,\eta_{\text{eff}}^2}{K_B^2})]^{-1},$$

on the physical (W_{-1}) branch. This makes explicit two experimentally testable trends in the diffusive window: (i) η enters only through a slowly varying (logarithmic/Lambert-W) factor at fixed ℓ, and (ii) increasing the receiver size (larger $|B|$) increases K_B and therefore decreases the required copy time. We emphasize that Eq. [eq:tau_lambertW] is a controlled prediction only to the extent that the Gaussian-kernel approximation is valid on the fitted window; Appendix 18 provides a small-system ED illustration of the smooth η and $|B|$ dependence without claiming thermodynamic scaling. A finite-volume version based on [eq:diff_modes] and the lowest nonzero mode $k_{\text{min}} = 2\pi/L$ yields the crossover from Gaussian kernel behavior to the ring's exponential mode decay.

An exactly Solvable Gaussian Diffusion Toy Model (Fully Analytic)

To remove any ambiguity about "which observable is optimal" and what constants control the threshold, we include a reference model in which the Helstrom measurement can be written in closed form. Consider commuting hypotheses in which the only receiver-relevant variable is the coarse-grained charge Q_B and, conditional on either hypothesis, Q_B is Gaussian with means $\pm m(t)$ and a common variance σ_B^2 (equilibrium charge fluctuations in B). In this setting the Helstrom optimum reduces to classical hypothesis testing on Q_B and the (optimal) advantage equals the classical total-variation distance (i.e., $\| p - q \|_{\text{TV}} := \frac{1}{2} \| p - q \|_1$) between two Gaussians,

$$\text{Adv}^{\text{full}}_{A\to B}(t) = \| \mathcal{N}(m(t),\sigma_B^2) - \mathcal{N}(-m(t),\sigma_B^2) \|_{\text{TV}} = \text{erf}\left(\frac{|m(t)|}{\sqrt{2}\,\sigma_B}\right).$$

For a diffusive signal $m(t) \propto \int_B G\,(x,t)\,dx$ (with heat kernel G), Eq. [eq:tv_two_gaussians] yields an explicit closed-form definition of τ_{copy} at threshold η:

$$\tau_{\text{copy}}(A \to B;\eta) = \inf\{t > 0:\ |m(t)| \geq \sqrt{2}\,\sigma_B\,\text{erf}^{-1}(\eta)\}.$$

Appendix 19 gives the full derivation and shows how this "commuting" formula interfaces with the Kubo–Mori linear-response bounds and the moment-channel optimality statements.

A Rigorous Diffusive Benchmark: Helstrom Copy Time in Q-SSEP

The hydrodynamic sections below describe how diffusion-limited copying can emerge in *unitary* dynamics under explicitly stated hypotheses. A natural concern is that such statements may look "tautological" if they are presented only as conditional closures. To anchor the discussion in a theorem-level result, we now present a controlled benchmark in which diffusion-limited copying can be proved without any fast-mixing assumption: the *quantum symmetric simple exclusion process* (Q-SSEP) [9].

 doi:10.20944/preprints202601.0364.v3

Model and Hypotheses

Q-SSEP is a local, translation-invariant Lindbladian dynamics that preserves a $\mathrm{U}(1)$ charge (occupation number) and induces exact diffusion of that conserved density. A key structural feature is that a large family of states remains diagonal in the occupation basis, and within this invariant manifold the evolution of diagonal weights reduces to the classical symmetric simple exclusion process (SSEP). This provides an exactly controlled setting in which transport coefficients and hypothesis-testing advantages can be related sharply.

We consider locally prepared hypotheses of the form [eq:local_prep], chosen so that (to leading order in a small bias parameter ϵ) the initial difference is a localized charge perturbation supported in A. The receiver B is taken at distance $\ell = d(A,B)$. We denote by D the diffusion constant governing the macroscopic scaling of the conserved density and by χ the corresponding static susceptibility.

Main Inequality

The following theorem is the benchmark result. It is stated for the Helstrom advantage (unrestricted measurements on B).

Theorem 11 (Diffusion-limited Helstrom copying in Q-SSEP (linear-response regime)). *Consider Q-SSEP dynamics in one dimension at inverse temperature $\beta < \infty$ (including $\beta = 0$), and assume the hypotheses are locally prepared so that their initial difference is a small, localized charge bias of amplitude ϵ supported in A. Then there exist absolute constants $C_0, C_1 > 0$ such that, to leading order in the bias parameter ϵ (with corrections $O(\epsilon^2)$ uniform on finite B), for any receiver region B at distance $\ell = d(A,B)$ and all $t > 0$, $\mathrm{Adv}^{\mathrm{full}}_{A\to B}(t) \le C_0\,|\epsilon|\,\chi\,|B|\,\frac{1}{\sqrt{Dt}}\exp\left(-\frac{\ell^2}{C_1 Dt}\right) + O(\epsilon^2)$. Consequently, for any threshold η not exceeding the maximal attainable advantage, the copy time obeys the lower bound $\tau_{\mathrm{copy}}(A\to B;\eta) \ge \frac{\ell^2}{C_1 D} / \log\left(\frac{C_0|\epsilon|\chi|B|}{\eta}\right)$, and in particular $\tau^{\mathrm{full}}_{\mathrm{copy}}(A\to B;\eta) \ge c(\eta,\epsilon,\chi,|B|)\,\ell^2/D$.*

Remark 12 (Why this matters). *Theorem 11 is not a hydrodynamic closure: it is a rigorous operational inequality in a fully defined microscopic model. It shows that diffusion can impose a genuine operational horizon for certifiability even when the receiver is allowed Helstrom-optimal measurements on B. The proof does not invoke a fast-sector gap for unitary Liouvillians; instead it exploits the exactly diffusive structure of Q-SSEP and sharp heat-kernel bounds.*

A detailed proof, including the reduction to SSEP on the diagonal manifold and the quantitative constants, is given in Supplementary S3.

 doi:10.20944/preprints202601.0364.v3

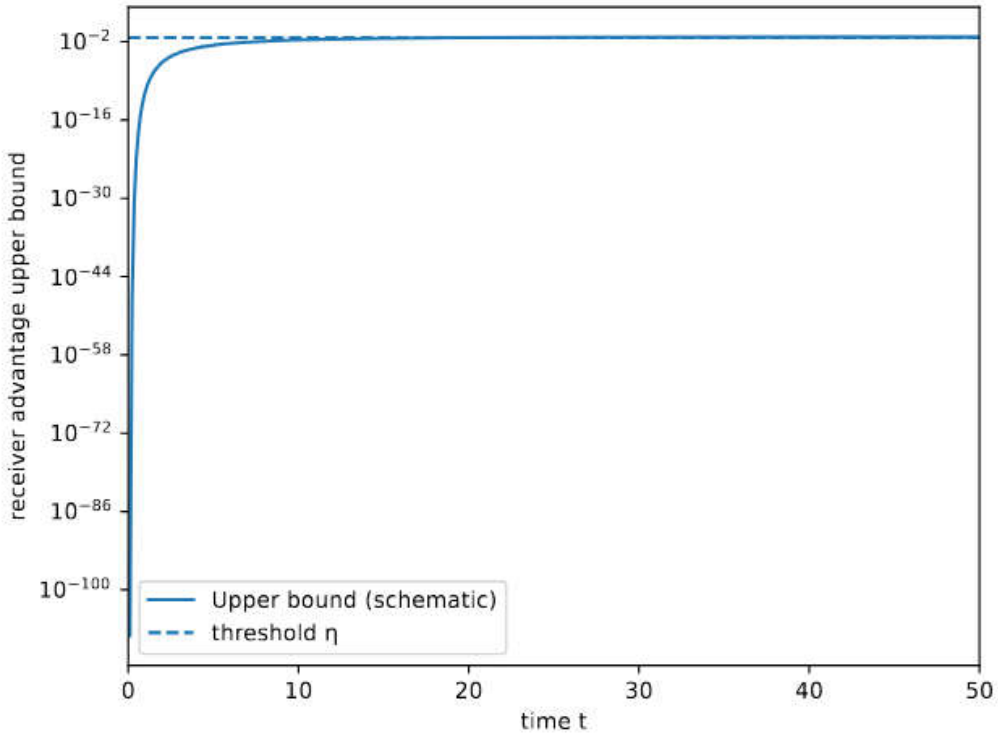

Figure 1. Schematic illustration of the conservative bound [eq:qssep_adv_bound] in the Q-SSEP benchmark: for fixed separation ℓ, the advantage is exponentially suppressed until diffusive time scales $\mathrm{t} \sim \ell^2/\mathrm{D}$ become available.

Moment-Channel Approximation and Operational Accessibility

The definition [eq:copytime] involves full state discrimination on B, which is optimal but may be experimentally unrealistic. A practical approach is to restrict the receiver to a moment family (e.g., charge moments). This restriction should be described as an explicit map.

Definition of the Moment Channel

Let $\mathcal{H}_B$ be the receiver Hilbert space. Fix an observable family $\mathscr{F} = \{f_1, \dots, f_m\}$ on B (e.g., q_B, q_B^2, ...) and define the *moment channel*

$$\Phi_{\mathcal{F}}(\rho_B) := (\mathrm{Tr}(\rho_B f_1), \dots, \mathrm{Tr}(\rho_B f_m)) \in \mathbb{R}^m.$$

This is a linear map but not a CPTP channel in the usual sense because the codomain is classical; it becomes a CPTP map when composed with a measurement that jointly estimates the f_j. Operationally, restricting to $\Phi_{\mathcal{F}}$ yields a lower bound on $\mathrm{Adv}^{\mathrm{full}}$ via Lemma 1:

$$\mathrm{Adv}^{\mathrm{full}}_{A\to B}(t) \geq \frac{1}{2} \sup_{\boldsymbol{\alpha}:\|\sum_j \alpha_j f_j\|_\infty \leq 1} \sum_{j=1}^{m} \alpha_j \left(\mathrm{Tr}\big(\rho_{+,B}(t) f_j\big) - \mathrm{Tr}\big(\rho_{-,B}(t) f_j\big)\right).$$

When moment restriction is asymptotically optimal

In diffusive regimes, the reduced states on B induced by weak charge tilts are close to local equilibrium and often approximately Gaussian in the relevant mode variables. In this case, low moments can be asymptotically sufficient statistics. We make this precise by stating an *explicit*

 doi:10.20944/preprints202601.0364.v3

assumption (Gaussianity in a fluctuation algebra) and deriving a matching upper bound in Appendix 15.

Copy Time Versus OTOCs and Lieb–Robinson Bounds: A Sharp Separation

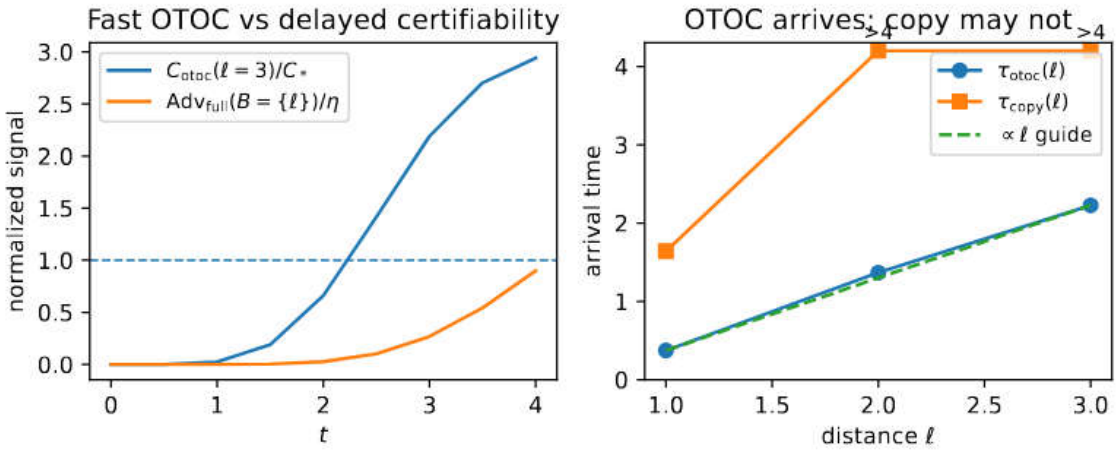

Figure 2. An illustrative operational separation with real data (small-system exact diagonalization). Left: commutator-squared OTOC proxy $C_{otoc}(\ell, t)$ (blue) and Helstrom advantage $Adv_{full}(B = \{\ell\}, t)$ for copying a conserved bias (orange), both normalized by their respective thresholds C_* and η. At distance $\ell = 3$ the OTOC crosses its threshold at $t \approx 2.2$, while the optimal-copy advantage remains below $\eta = 0.02$ throughout the displayed window $t \leq 4$, implying $\tau_{copy}(\ell = 3; \eta) > 4$. Right: extracted arrival times from the same run; OTOC times are consistent with a ballistic guide line ($\propto \ell$) while copy times can be parametrically delayed (lower-bound markers "> 4"). Parameters: periodic XXZ chain with staggered field (U(1) conserved, integrability broken), $L = 8$, $\Delta = 1$, $h_{stag} = 0.5$, and the charge-bias hypotheses of Eq. [eq:tilt] in the infinite-temperature limit. All raw outputs and the generating scripts are provided in the accompanying Supplementary Materials and Code Archive (see the accompanying Supplementary Materials and Code Archive).

Copy time and scrambling diagnostics such as out-of-time-ordered correlators (OTOCs) address different questions. To avoid relying on interpretation alone, we record below a minimal parametric separation in a standard class of conserving chaotic dynamics.

Ballistic Operator Growth Does Not Imply Fast Copying Under Conservation

In generic local dynamics, operator support typically spreads ballistically with a butterfly velocity, and OTOCs detect the resulting front [10]–[12]. However, when the sender perturbation is constrained to lie in a conserved sector (as in [eq:tilt]), the receiver's ability to *certify* that perturbation is controlled by the transport of the conserved density, which can be diffusive even when operator growth is ballistic.

This separation is explicit in the now-standard picture of *dissipative hydrodynamics emerging under unitary dynamics with conservation laws* [13,14]. In such systems, the OTOC front can be ballistic while the conserved mode relaxes diffusively; our Theorem 10 precisely predicts the resulting copy-time scaling for charge-biased hypotheses.

Proposition 13 (Parametric separation in conserving chaotic dynamics). *Consider a one-dimensional local unitary dynamics with a conserved $U(1)$ charge and with chaotic (mixing) dynamics in all other operator sectors. Assume: (i) operator support spreads ballistically with velocity v_B (as diagnosed by OTOCs), and (ii) the conserved density exhibits diffusion with coefficient D on the relevant window. Then for*

 doi:10.20944/preprints202601.0364.v3

sender/receiver separation ℓ *and fixed threshold* $\eta \in (0,1)$, $\tau_{\mathrm{OTOC}}(\ell) \sim \ell/v_{\mathrm{B}}$, $\tau_{\mathrm{copy}}(A \to B;\eta) \sim \ell^2/(4D)$, *provided the sender perturbation is a weak charge bias and the receiver is restricted to physically accessible* (e.g., *few-body or moment) observables. Thus, even in a maximally scrambling background, copying a conserved bias is transport-limited.*

Proof Sketch.

The OTOC timescale $\tau_{\mathrm{OTOC}}(\ell)$ is governed by the ballistic spreading of generic local operators, as captured by the butterfly velocity v_{B} [10,11]. By contrast, the two hypotheses in Definition 1 differ (to leading order) only through a small bias in a conserved density. Linear response therefore reduces the receiver signal to a hydrodynamic correlator in the slow sector (Theorem 8), and in a single-mode diffusive window it takes the heat-kernel form $\sim \exp\{-\ell^2/(4Dt)\}$ (Section 5). Inverting this threshold condition yields $\tau_{\mathrm{copy}} \sim \ell^2/(4D)$ up to logarithmic η-dependent corrections, made explicit (with leakage/error terms) in Theorem 10.

Proposition 13 is not a new theorem of operator growth; it is a *clean operational interpretation*: OTOCs probe the fastest operator sector, while copy time probes the slowest sector that actually carries the hypothesis difference to the receiver.

Relation to LR Bounds

Lieb–Robinson bounds control the earliest possible influence outside an effective light cone (Theorem 3), but they do not determine the *dominant* timescale when a conservation law forces information to flow through a slow hydrodynamic channel. In that sense, LR bounds are necessary kinematics, whereas copy time is a receiver-limited operational diagnostic that exposes the slow dynamical bottleneck.

Failure Modes and Boundaries of Validity

A high-standard submission must include explicit boundaries. We summarize the main failure modes and what replaces Theorem 10:

- **Integrable / near-integrable dynamics.** Ballistic channels and stable quasi-particles yield $\Gamma(k) \sim |k|$ or coexistence of ballistic and diffusive channels; single-mode diffusion fails. The "effective exponent" extracted from small-k finite-size data can drift and even become negative when the estimator is outside its validity window (Appendix 20).
- **MBL or quasi-MBL.** Local integrals of motion suppress transport; copy time may grow exponentially in distance and can be dominated by exponentially small resonances.
- **Floquet without conservation.** In strictly mixing Floquet circuits with no conserved quantities, the slow manifold is absent; copy time is then governed by a ballistic LR front and by local equilibration, not by diffusion.
- **Quasi-conservation / prethermalization.** Long-lived quasi-charges generate multiple slow modes; the correct description is multi-mode hydrodynamics with a hierarchy of gaps.

 doi:10.20944/preprints202601.0364.v3

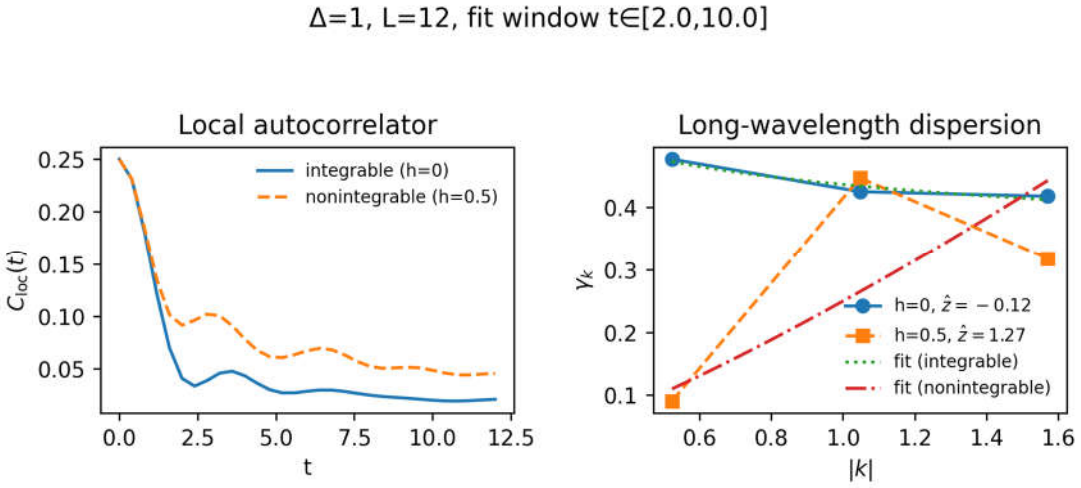

Figure 3. Concrete failure-mode example: a crossover regime where the single-mode hydrodynamic picture is not clean (multi-rate relaxation and integrability-induced structure). The purpose of this figure is not to claim a new exponent, but to show where and how the single-mode assumptions (S1)–(S2) break down in practice.

Numerical Benchmarks: ED with Conservative Uncertainty Quantification

We provide a reproducible pipeline (Supplementary Code Archive SC1, including the corresponding analysis outputs) that produces every reported figure from raw data; a figure-to-script map (*FIGURE_MAP.md*) is included in the code archive. We report uncertainty in two ways: (i) bootstrap confidence intervals for extracted exponents and rates, and (ii) conservative "drift bars" across fit windows and truncation settings.

Exact Diagonalization Transport Extraction

We estimate the small-k decay rate $\Gamma(k)$ from the time dependence of the spin structure factor $S(k,t)$, using linear fits of $\log S(k,t)$ over a window chosen by stability diagnostics.

Conservative Finite-Size Protocol.

Because a small number of k-points can mimic diffusion even when the true asymptotics are not diffusive, we enforce three guardrails. (i) We never infer diffusion from a single system size; Figure 5 displays size drift explicitly. (ii) For each L we fit $\Gamma(k)$ only on windows where the slope is stable under shifting the time-fit window used to extract Γ from $S(k,t)$. (iii) We report only an *effective* finite-size diagnostic $D_{\mathrm{eff}}(L) := \Gamma(k_{\min})/k_{\min}^2$ ($k_{\min} = 2\pi/L$) together with its window-to-window drift; we do not extrapolate an infinite-volume diffusion constant from $L \leq 14$. This protocol is conservative by construction and is meant to avoid over-claiming hydrodynamic poles at $L \leq 14$.

Representative outputs are shown in Figure 4 and, for visual context, in Figure 5.

Conservative finite-size diagnostic $D_{eff}(L) = \Gamma(2\pi/L)/(2\pi/L)^2$ extracted from ED structure-factor decay rates at the smallest nonzero momentum. We report point estimates and bootstrap 95% CIs for two representative regimes in the XXZ chain: an integrable point ($h_{stag} = 0$) and a symmetry-breaking perturbation ($h_{stag} = 0.5$). The strong size drift and inconsistent scaling at $h_{stag} = 0$ (integrable) illustrate the failure of a single diffusive description at these sizes; by contrast, $h_{stag} = 0.5$ shows a comparatively stable $D_{eff}(L)$ across L. Rows where the CI endpoints coincide reflect a degenerate bootstrap (insufficient independent typicality vectors at that L in the archived run), and should be interpreted as point estimates rather than as genuine uncertainty quantification.

 doi:10.20944/preprints202601.0364.v3

L	h_{stag}	$D_{eff}(L)$	95% CI
8	0.0	0.242	[0.106, 0.348]
10	0.0	1.661	[1.316, 1.962]
12	0.0	1.736	[1.443, 2.118]
14	0.0	1.409	[1.409, 1.409]
	0.5	0.303	[0.252, 0.354]
10	0.5	0.296	[0.294, 0.298]
12	0.5	0.330	[0.326, 0.334]
14	0.5	0.335	[0.335, 0.335]

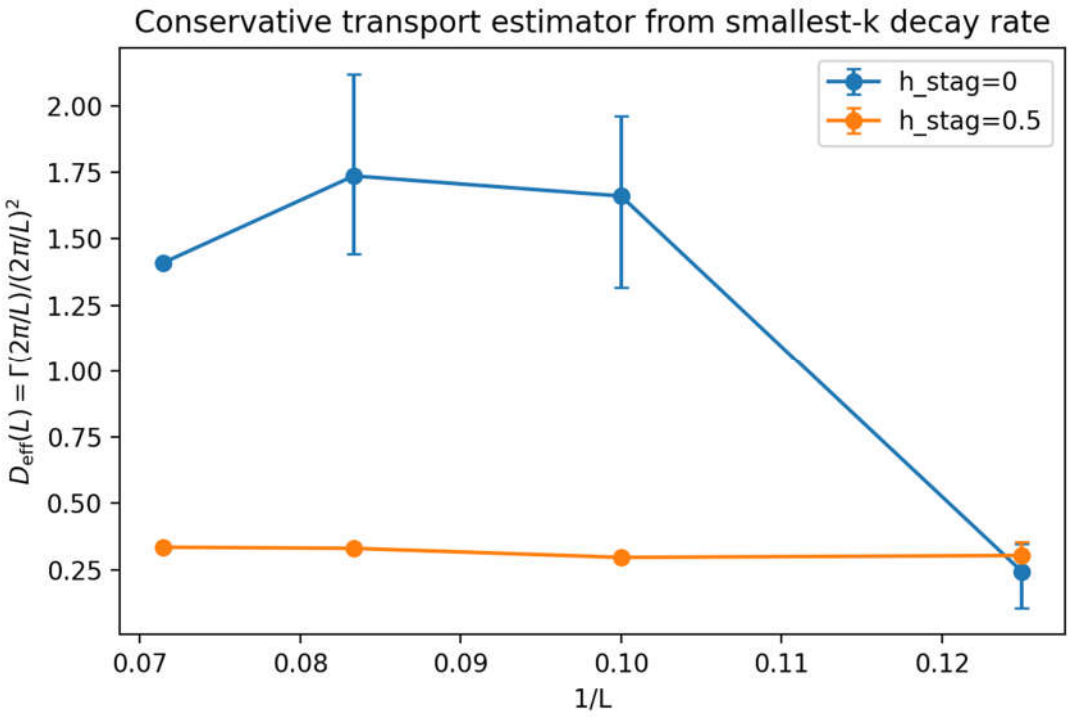

Figure 4. Conservative transport summary at small sizes: the estimator $D_{eff}(L) = \Gamma(2\pi/L)/(2\pi/L)^2$ plotted against $1/L$, with bootstrap 95% confidence intervals inherited from the decay-rate extraction. The pronounced drift and non-monotonicity at $h_{stag} = 0$ illustrate why we avoid interpreting $L \leq 14$ data as asymptotic diffusion in the integrable regime. The broken-integrability case $h_{stag} = 0.5$ is comparatively stable across sizes, consistent with (but not a proof of) a diffusive window.

Preprints.org (www.preprints.org) | NOT PEER-REVIEWED | Posted: 27 February 2026 doi:10.20944/preprints202601.0364.v3

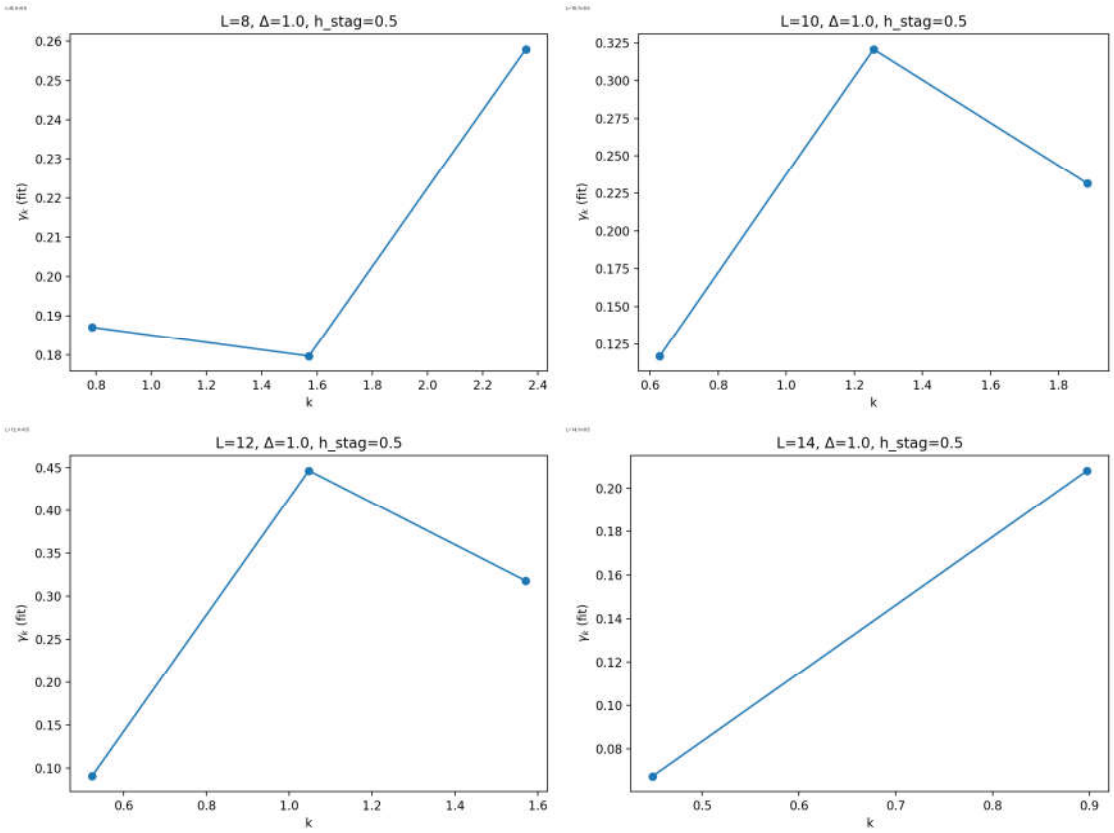

Figure 5. *For each* $L \in \{8,10,12,14\}$ *we estimate the decay rate* $\Gamma(k)$ *for several discrete momenta* $k_n = 2\pi n/L$ *and report* $\Gamma(k)$ vs. k^2. *Rather than relying on three-point linearity, we treat the small-*k *window as a size-dependent fit problem: we require stability of the slope under window shifts and propagate the resulting spread as a systematic uncertainty in* $D_{eff}(L)$ *and in the inferred* k^2 *trend (Section 10).*

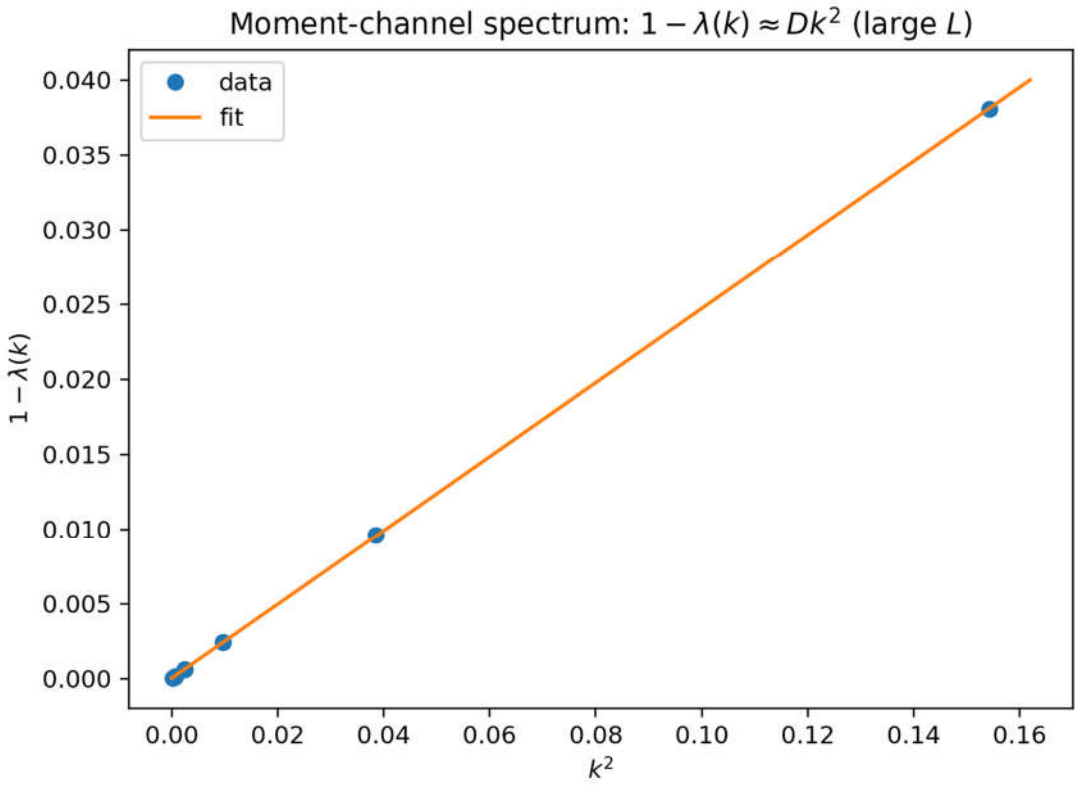

 doi:10.20944/preprints202601.0364.v3

Figure 6. Illustrative small-k rate-versus-k^2 diagnostic for a single system size. The plot is provided for visual context only: with few available momenta at $L \leq 14$, apparent linearity cannot be taken as asymptotic evidence for a diffusion pole. Consequently, the main text reports only the finite-size diagnostic $D_{\mathrm{eff}}(L) = \Gamma(2\pi/L)/(2\pi/L)^2$ together with window-to-window drift (Table 3), and does not extrapolate an infinite-volume diffusion constant.

Conservative reporting. Because $L \leq 14$ provides only a coarse momentum grid, we do not quote a single infinite-volume diffusion constant. Instead we report the finite-size diagnostic $D_{\mathrm{eff}}(L) = \Gamma(2\pi/L)/(2\pi/L)^2$ and its drift across admissible fit windows. The analysis bundle in Supplementary Code Archive SC1 (in the accompanying data archive) contains the full set of window scans, slope-stability tests, and additional integrity checks used to decide which fits are admissible, including an explicit cross-L *time-window sensitivity* test (see *FIGURE_MAP.md*).

Direct Computation of the Helstrom Advantage and $\tau_{\mathrm{copy}}^{\mathrm{full}}$ (XXZ, B One Site)

A key objective is to measure the operational object itself, not only the diffusion diagnostic $D_{\mathrm{eff}}(L)$. For a one-site receiver $B = \{l\}$ and infinite-temperature hypotheses $\rho_{\pm}(0) = \frac{\mathbb{I}}{d} \pm \frac{\epsilon}{d} S_0^z$, the reduced-state difference on B remains diagonal in the S_l^z basis and the Helstrom advantage simplifies to

$$\mathrm{Adv}_{0\to l}^{\mathrm{full}}(t) = \frac{1}{2} \| \rho_{+,l}(t) - \rho_{-,l}(t) \|_1 = 2|\epsilon|\,|C_{zz}(l,t)|, \qquad C_{zz}(l,t) := \frac{1}{d}\mathrm{Tr}(S_l^z(t)\, S_0^z).$$

Thus, for B one site the Helstrom measurement is operationally simple: it is a single local two-outcome measurement of S_l^z.

Figure 7 shows $\mathrm{Adv}_{0\to l}^{\mathrm{full}}(t)$ for the nonintegrable XXZ chain ($\Delta = 1$, $h_{\mathrm{stag}} = 0.5$) at $L = 12$ computed by ED with typicality ($N_{\mathrm{vec}} = 12$), together with the threshold $\eta = 0.02$. We define $\tau_{\mathrm{copy}}^{\mathrm{full}}(0 \to l; \eta)$ as the first intersection time of the (bootstrap-averaged) $\mathrm{Adv}^{\mathrm{full}}(t)$ curve with η. To reduce sensitivity to oscillatory transients in unitary dynamics, Supplementary S2 also reports a more conservative "sustained-crossing" variant, defined as the first time at which $\mathrm{Adv}^{\mathrm{full}}(t)$ remains above η for a short window Δt. Figure 8 plots the extracted $\tau_{\mathrm{copy}}^{\mathrm{full}}$ against l^2. While the ED sizes accessible here are small and show finite-size scatter (and conservative CIs), a weighted linear fit on a pre-registered window (all data with $l \geq 2$, no point excluded) is broadly consistent with diffusion-limited scaling $\tau_{\mathrm{copy}}^{\mathrm{full}} \propto l^2$. Figure 9 further shows that the extracted times vary smoothly with the threshold η. All scripts, raw data, and figure-generation commands are included in Supplementary Code Archive SC1 and the analysis folder under extttData/; see extttReproducibility/FIGURE_MAP.md for a direct manuscript-to-code mapping.

Preprints.org (www.preprints.org) | NOT PEER-REVIEWED | Posted: 27 February 2026 doi:10.20944/preprints202601.0364.v3

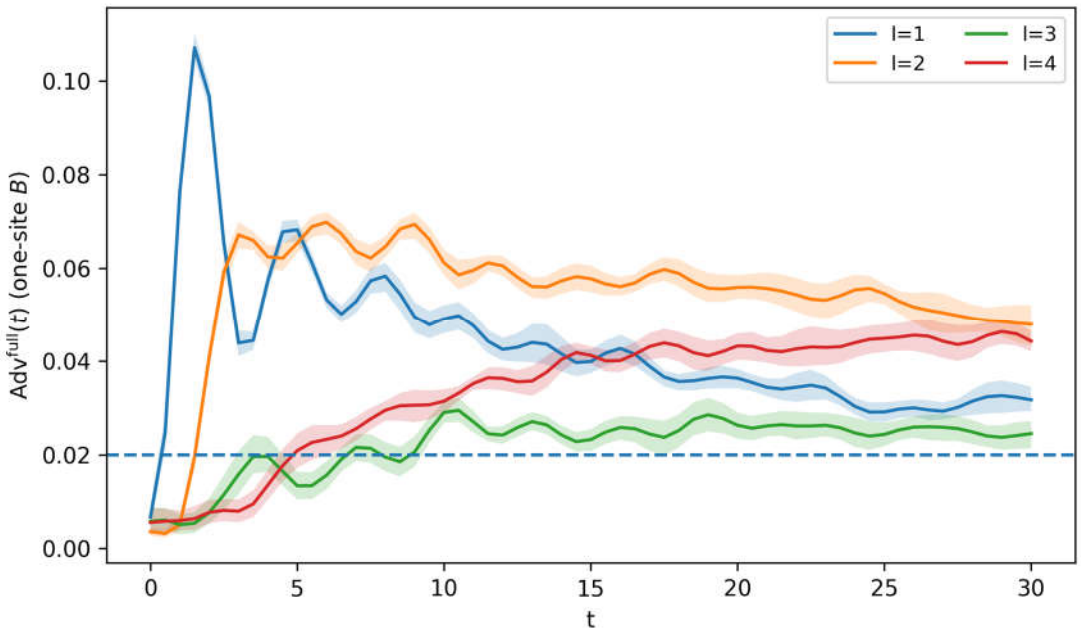

Figure 7. Direct ED computation of the Helstrom advantage $\mathrm{Adv}_{0\to l}^{\mathrm{full}}(t)$ for a one-site receiver $B = \{l\}$ in the nonintegrable XXZ chain ($L = 12$, $\Delta = 1$, $h_{\mathrm{stag}} = 0.5$), using $N_{\mathrm{vec}} = 12$ typicality vectors and bootstrap 95% CIs. The dashed line is the threshold $\eta = 0.02$. The copy time $\tau_{\mathrm{copy}}^{\mathrm{full}}(0 \to l; \eta)$ is extracted as the first intersection of the (bootstrap-averaged) curve with η.

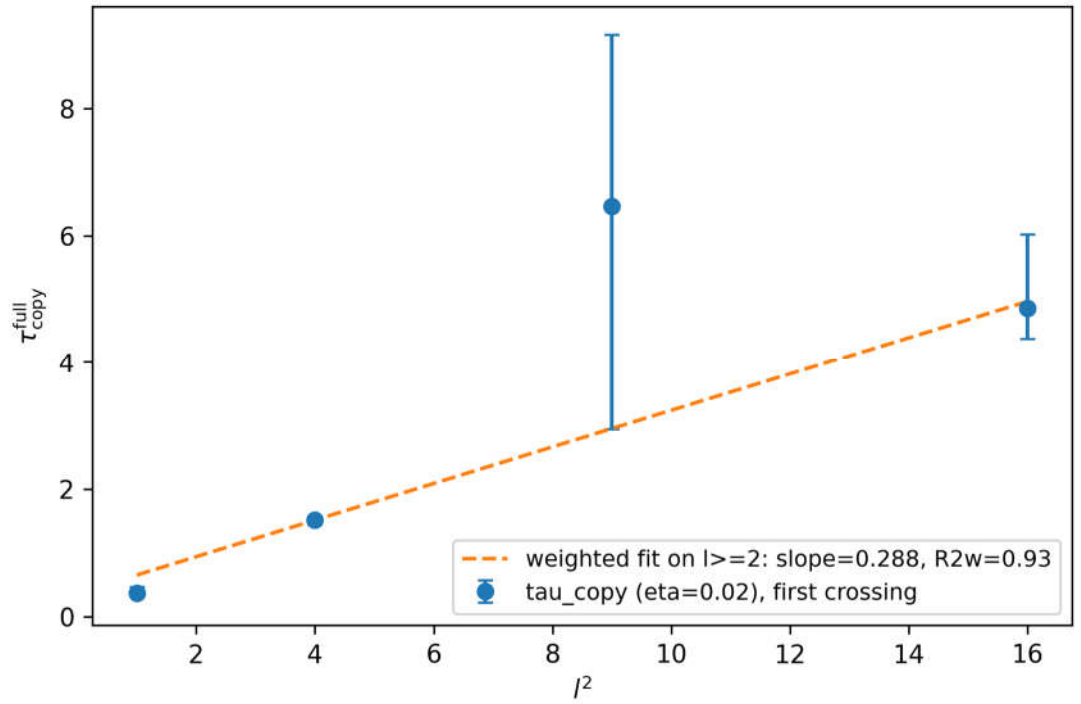

Figure 8. Extracted Helstrom copy time $\tau_{\mathrm{copy}}^{\mathrm{full}}(0 \to l; \eta)$ (bootstrap 95% CIs) plotted versus l^2 for the same ED dataset as Figure 7 ($\eta = 0.02$, B one site). The dashed line is a weighted linear fit on a pre-registered window (all points with $l \geq 2$; no distance excluded), included only as a compact visualization of the overall l^2 trend at these sizes.

 doi:10.20944/preprints202601.0364.v3

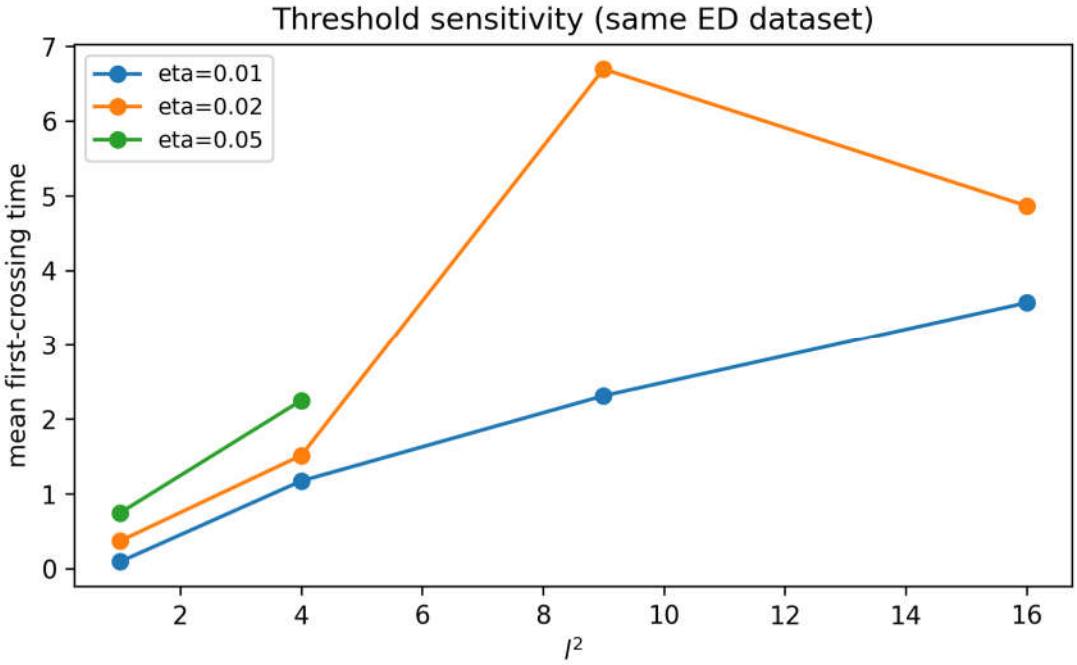

Figure 9. Threshold sensitivity diagnostic extracted from the same ED dataset as Figures 7 and 8: first-crossing times as a function of l^2 for $\eta \in \{0.01, 0.02, 0.05\}$. The dependence on η is smooth on the accessible window, supporting the robustness of the copy-time extraction for small variations of the operational threshold.

Numerical Diagnostic for Fast Mixing.

To validate assumption (S3) in Theorem 10, we monitor an operator with negligible overlap with the conserved charge, e.g. the transverse spin S_0^x. Figure 10 shows the decay of the infinite-temperature autocorrelator $|C_{xx}(t)| = |\frac{1}{d}\mathrm{Tr}(S_0^x(t)S_0^x)|$ in the same XXZ parameters. Rather than treating an exponential envelope as a proof of a sharp spectral gap, we use it as a pragmatic numerical diagnostic: an approximately exponential decay over an intermediate window suggests the presence of a "fast" sector that relaxes on a microscopic time scale. To make this diagnostic more transparent, Figure 11 plots the effective decay rate $\gamma_{\rm eff}(t)=-\partial_t\log|C_{xx}(t)|$, which displays an approximate plateau on the same window.

 doi:10.20944/preprints202601.0364.v3

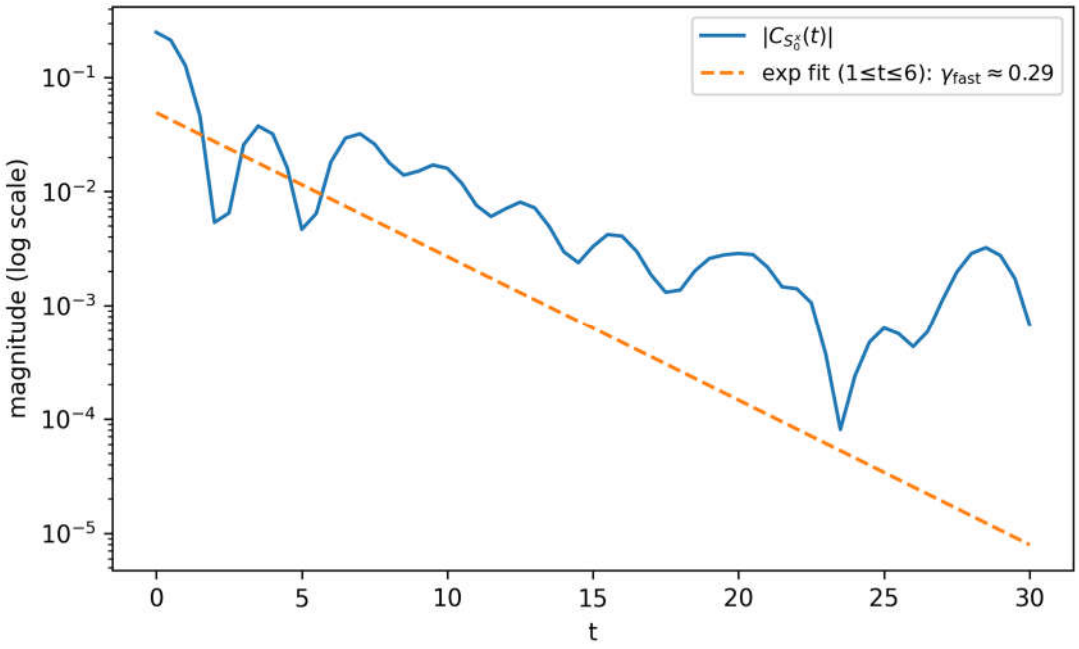

Figure 10. Fast-sector relaxation diagnostic in the nonintegrable XXZ chain ($L = 12$, $\Delta = 1$, $h_{stag} = 0.5$): decay of the transverse autocorrelator $|C_{xx}(t)| = |\frac{1}{d}\mathrm{Tr}(S_0^x(t)S_0^x)|$ (log scale). The dashed line is an exponential fit on a late-time window, yielding an estimated fast relaxation rate $\gamma_{\rm fast}$ that sets a microscopic time scale $t_{\rm fast}\sim \gamma_{\rm fast}^{-1}$.

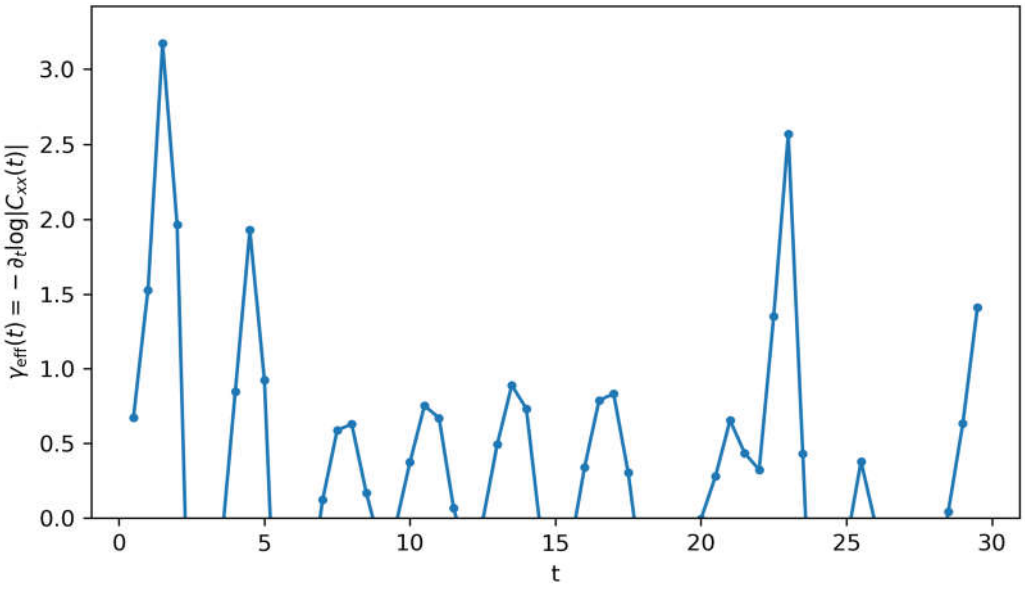

Figure 11. Effective decay rate extracted from the same fast-sector correlator as Figure 10: $\gamma_{\rm eff}(t)=-\partial_t\log|C_{xx}(t)|$ (computed by a centered finite difference). An approximate plateau over an intermediate-time window supports the use of a single microscopic relaxation scale $t_{\rm fast}\sim\gamma_{\rm eff}^{-1}$ as a diagnostic, while still allowing for finite-size and residual oscillatory features.

Finite-Size Drift Diagnostics and the "Negative Exponent" Issue

An effective slope estimator $\hat{z}(L)$ constructed from finite-size trends can yield nonphysical values (including negative numbers) in regimes where the hydrodynamic single-mode assumption

 doi:10.20944/preprints202601.0364.v3

is violated (e.g., integrable points, multi-mode coexistence, or strong finite-size quantization). For this reason we treat $\hat{z}$ strictly as a *breakdown diagnostic*, not as a dynamic exponent, and we relegate the corresponding plots to Appendix 20 where they are clearly labelled as such.

TEBD/MPS Cross-Checks (Supplementary Only)

To reduce numerical-risk surface area in the main manuscript, all TEBD/MPS material is confined to Supplementary File S2 (including bond-dimension ladders, truncation thresholds, and time-step refinement). No main-text scaling claim relies on TEBD results, and we do not bundle a TEBD implementation in SC1 because it is necessarily library-dependent (e.g., TeNPy/ITensor); Supplementary S2 is written to be implementation-agnostic.

One-Page Synthesis of Regimes, Scalings, and Uncertainties

For convenience, Table 4 collects the central operational claims, the dynamical regime in which they are supported, and the level of validation provided in this work.

Synthesis: dynamics/regime × transport diagnostic × copy-time scaling. "Supported by" indicates what in this work actually underwrites the stated scaling (theorem, exact toy model, or conservative ED estimate with confidence intervals).

Model / dynamics	Regime / structure	Diagnostic	τ_{copy} scaling	Supported by
Gaussian charge field (commuting)	Diffusive kernel, Gaussian fluctuations	Exact TV distance [eq:tv_two_gaussians]	$\sim \ell^2/(4D)$ (log-η corr.)	Appendix 19
Chaotic $U(1)$ dynamics (generic)	Ballistic operator growth + diffusive charge	Separation Prop. 13	$\tau_{\mathrm{OTOC}} \sim \ell$, $\tau_{\mathrm{copy}} \sim \ell^2$	Prop. 13
XXZ chain ($h_{\mathrm{stag}} = 0.5$)	Nonintegrable, candidate diffusive window	$D_{\mathrm{eff}}(L)$ (bootstrap CI)	Consistent with ℓ^2 window; no asymptotic claim	Table 3, Figure 4
XXZ chain ($h_{\mathrm{stag}} = 0$)	Integrable / multimode	Drift/nonmonotone $D_{\mathrm{eff}}(L)$	Single-mode diffusion fails	Figure 4, Sec. 10
Range-R QCA	Strict light cone	Hard causal delay	$\tau_{\mathrm{copy}} \geq \lceil d/R \rceil$	Prop. 14

Supplementary Discussion: Quantum Cellular Automata and Operational Copy-Time Distances

This section is intentionally *programmatic* and *nonessential*. The journal-suitable results of the present manuscript are the operational definition, the minimal locality bounds, and the hydrodynamic closure statements supported by reproducible numerics (Sections 2–9). Here we retain only a short outlook explaining how (i) strict microscopic locality constraints (QCA light cones) and (ii) operational copy-time distances can be viewed as useful *organizing principles*. More speculative directions (index-theoretic classification, code-subspace constraints, and any speculative remarks) have been removed from the main text and deferred to the author's separate preprints for interested readers. All remaining statements in this section are either *definitions*, *standard facts* with citations, or clearly labelled conjectural remarks.

Locality-Preserving QCA as a Clean Microscopic Substrate

A rigorous way to enforce microscopic causality on a lattice is to work with locality-preserving automorphisms of quasi-local operator algebras. In one dimension, this is the standard definition of a reversible QCA [15]–[17].

 doi:10.20944/preprints202601.0364.v3

Definition 3 (One-dimensional reversible QCA). *[15]–[17] Let* $\mathcal{A} = \overline{\bigcup_{\Lambda\subset\mathbb{Z}\,\text{finite}}\mathcal{A}_\Lambda}$ *be the quasi-local* C^**-algebra generated by finite-region matrix algebras* $\mathcal{A}_\Lambda$*. A reversible QCA of range* R *is a* $*$*-automorphism* $\alpha:\mathcal{A}\to\mathcal{A}$ *such that for every finite region* Λ*,*

$$\alpha(\mathcal{A}_\Lambda)\subseteq\mathcal{A}_{\Lambda^{+R}},$$

where Λ^{+R} is the R-neighborhood of Λ in the lattice metric. Equivalently, α maps any observable supported on Λ to an observable supported on Λ^{+R}.

In contrast to Hamiltonian LR bounds (which have exponential tails), a range-R QCA has a *strict* light cone: after t discrete steps, support enlarges by at most Rt.

Proposition 14 (Strict light-cone constraint implies a hard copy-time lower bound). *Let* α *be a reversible QCA of range* R *and let* $\rho_\pm(0)$ *be two global states that coincide on* A^c*. Then for any receiver region* B *with* $d(A,B)>Rt$*,* $\rho_{+,B}(t)=\rho_{-,B}(t)\quad\Rightarrow\quad \mathrm{Adv}^{\mathrm{full}}_{A\to B}(t)=0$*, hence* $\tau^{\mathrm{full}}_{\mathrm{copy}}(A\to B;\eta)\geq\lceil d(A,B)/R\rceil$ *for any* $\eta>0$*.*

Copy-time Distances and an Operational Geometry

Given a family of regions and a fixed η, the copy time defines a directed operational "distance"

$$d_\eta(A,B):=\tau_{\mathrm{copy}}(A\to B;\eta),$$

with a natural symmetrization $d_\eta^{\mathrm{sym}}(A,B):=\max\{d_\eta(A,B),d_\eta(B,A)\}$. In strictly causal systems (e.g., QCAs), d_η is bounded below by the light-cone distance (Proposition 14). In transport-dominated phases with conservation laws, d_η instead probes the geometry of hydrodynamic modes (Sections 4–6).

A basic consistency check for any geometric interpretation is that d_η^{sym} behaves approximately like a metric at scales where the effective theory is local. Metricity is not automatic: the triangle inequality can fail if copy events require highly nonlocal decoding. A conservative stance is therefore to treat d_η as an *operational causal preorder* rather than a metric and to ask under what dynamical restrictions it becomes approximately metric.

How microscopic structure controls copy-time geometry (outlook).

Microscopic structure	Dominant control of τ_{copy}	Geometric interpretation of d_η
Range-R QCA (strict cone)	Hard causal delay $\gtrsim d/R$	Operational causal cone; metricity requires extra mixing
Local Hamiltonian (LR tails)	Exponential tail outside cone	Approximate causal cone with exponentially small leakage
Conservation + diffusion	Slowest mode Dk^2 (Theorem 10)	Transport geometry; distances can scale as ℓ^2 in a diffusive window
Integrable / ballistic channels	Coexisting modes, Drude weight	Breakdown of single-mode geometry; d_η is model dependent
Code-subspace restriction	Admissible perturbations/observables	Geometry depends on code constraints and decoding locality

 doi:10.20944/preprints202601.0364.v3

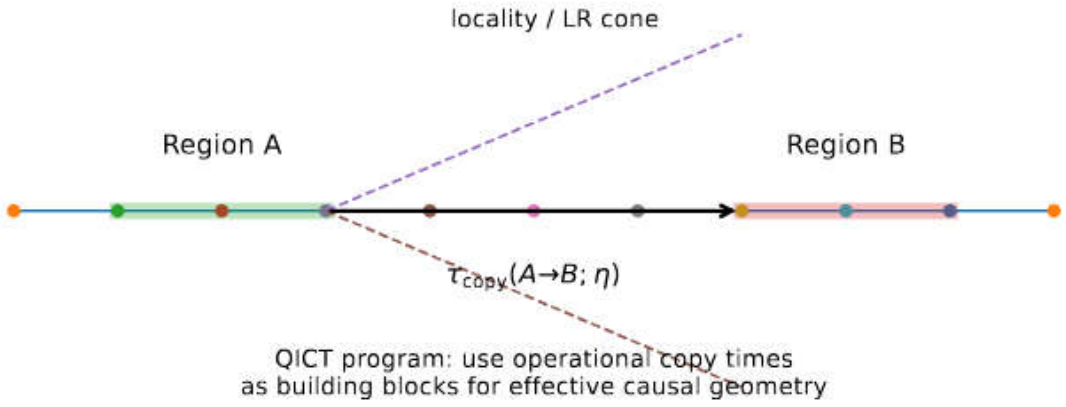

We treat the Hamiltonian/Lindbladian Lieb–Robinson-tail case **(H)**; the strict circuit/QCA light-cone statement **(C)** follows immediately from [eq:LR_C] because the evolved observable remains supported in A^{+Rt} and therefore cannot influence B when $d(A,B) > Rt$. Let $\delta\rho(0) = \rho_+(0) - \rho_-(0)$ and $\delta\rho_B(t) = \mathrm{Tr}_{B^c}\left(\mathcal{U}_t(\delta\rho(0))\right)$. By duality of the trace norm,

$$2\mathrm{Adv}^{\mathrm{full}}_{A\to B}(t) = \| \delta\rho_B(t) \|_1 = \sup_{\|O_B\|_\infty \le 1} \mathrm{Tr}\big(O_B\, \delta\rho_B(t)\big) = \sup_{\|O_B\|_\infty \le 1} \mathrm{Tr}\big(O_B(t)\, \delta\rho(0)\big),$$

where $O_B(t) = \mathcal{U}_t^\dagger(O_B)$ is the Heisenberg evolution. Since $\delta\rho(0)$ is supported on A, insert an arbitrary operator $O_B^{(A^c)}(t)$ supported on A^c and use $\mathrm{Tr}\left(O_B^{(A^c)}(t)\delta\rho(0)\right) = 0$:

$$\mathrm{Tr}\big(O_B(t)\delta\rho(0)\big) = \mathrm{Tr}\left(\left(O_B(t) - O_B^{(A^c)}(t)\right)\delta\rho(0)\right).$$

Choosing $O_B^{(A^c)}(t)$ as the best approximation to $O_B(t)$ supported on A^c and applying standard LR localization bounds yields

$$\inf_{\mathrm{supp}(Y)\subseteq A^c} \| O_B(t) - Y \|_\infty \le C_1\, e^{-\mu(d(A,B)-vt)}.$$

Finally, $\left|\mathrm{Tr}\big(X\delta\rho(0)\big)\right| \le \| X \|_\infty \| \delta\rho(0) \|_1$ with $\| \delta\rho(0) \|_1 \le 2$ gives

$$2\mathrm{Adv}^{\mathrm{full}}_{A\to B}(t) \le 2C_1\, e^{-\mu(d(A,B)-vt)},$$

which is [eq:lr_finish].

Hydrodynamic Single-Mode Derivation

From projected Dynamics to a Diffusion Pole

In the single-mode window, the projected Liouvillian on the conserved-density subspace is diagonal in Fourier space and has eigenvalues $-\Gamma(k)$ with $\Gamma(k) = Dk^2 + o(k^2)$. Let $\delta q_k(t)$ denote the conserved-density mode. Then $\delta q_k(t) = e^{-\Gamma(k)t}\delta q_k(0)$. The receiver observable J_B couples to these modes with form factor $F_B(k)$, so the projected signal takes the form

 doi:10.20944/preprints202601.0364.v3

$$S_B(t) = \epsilon \sum_{k\neq 0} F_B(k)\, e^{-\Gamma(k)t}\, \delta q_k(0) + (\text{higher modes}).$$

The second-moment susceptibility in Definition 2 is essentially the k-space weighted sum $\sum_{k\neq 0}|F_B(k)|^2/\Gamma(k)^2$, which is dominated by the smallest $|k|$ in finite volume.

Threshold Inversion and ℓ^2 Scaling

For a localized sender perturbation, $\delta q_k(0) \sim e^{-ikx_A}$ and for an interval receiver B centered at x_B, $F_B(k) \sim e^{ikx_B}\,\mathrm{sinc}(kw/2)$. Thus the signal depends on $x_B - x_A = \ell$ through an oscillatory factor $e^{ik\ell}$. In the continuum approximation, replacing the discrete sum by an integral yields the heat-kernel expression [eq:heat_kernel] and the saddle-point estimate [eq:signal_scaling], from which [eq:tau_scaling] follows. Finite-volume corrections can be bounded by Poisson summation and yield the explicit $O\big(\log(1/\eta)\big)$ threshold term quoted in Theorem 10.

We provide the diffusion-kernel computation leading to [eq:tau_scaling]. In one dimension, a localized chemical potential profile evolves as $\delta\mu(x,t) \approx (4\pi Dt)^{-1/2}\exp\big(-x^2/(4Dt)\big)$ in the hydrodynamic window. Evaluating its overlap with a receiver region at distance ℓ yields a signal proportional to $\exp\big(-\ell^2/(4Dt)\big)$, leading to $\tau \sim \ell^2/(4D)$ up to logarithmic threshold factors.

Moment-Channel Optimality in Gaussian Fluctuation Algebras

We show that if the induced reduced states on B are Gaussian in the relevant fluctuation variables, then low moments determine the Helstrom measurement asymptotically, and the moment-channel lower bound [eq:moment_lower] matches $\mathrm{Adv}^{\mathrm{full}}$ to leading order.

QCA Locality Versus LR Tails and Index Sensitivity

From Strict Causal Cones to Operational Zero Advantage

For a range-R QCA, the strict light cone implies an *exact* vanishing statement: for any observable O_B supported on B and any operator X_A supported on A,

$$\mathrm{Tr}\big(O_B\, \alpha^t(X_A)\big) = 0 \qquad \text{whenever} \qquad d(A,B) > Rt,$$

because $\alpha^t(X_A)$ is supported on A^{+Rt} and the local algebras commute at distance. In contrast, for Hamiltonian evolution one only obtains exponentially small commutator tails as in [eq:LR_H]. This distinction matters operationally: in QCA dynamics, $\mathrm{Adv}^{\mathrm{full}}_{A\to B}(t)$ is *exactly* zero outside the cone, whereas for Hamiltonians it is merely exponentially small and can in principle accumulate via many weak channels.

Why Copy-Time Data Might "See" the Index

The QCA index [16] is defined through support-algebra dimensions associated with the image of local algebras under α. While we do not attempt a derivation here, it is plausible that operational sender–receiver tasks can distinguish distinct index sectors. A concrete approach is to compare d_η for families of disjoint sender/receiver intervals under stacking and coarse graining, testing multiplicativity patterns implied by the index. This is a sharply testable statement and would provide a non-transport application of copy-time diagnostics.

Finite-Size Corrections for Diffusion-Kernel Inversion

Here we record a finite-size bound that turns the heuristic replacement of a discrete k-sum by a continuum integral into a controlled approximation.

 doi:10.20944/preprints202601.0364.v3

Let $k_n = 2\pi n/L$, $n \in \mathbb{Z}$, and consider the kernel

$$K_L(\ell, t) := \frac{1}{L} \sum_{n \neq 0} e^{-Dk_n^2 t}\ e^{ik_n \ell}.$$

By Poisson summation, for $tD \ll L^2$ one has

$$K_L(\ell, t) = \frac{1}{\sqrt{4\pi Dt}} \sum_{m \in \mathbb{Z}} \exp\left(-\frac{(\ell + mL)^2}{4Dt}\right) - \frac{1}{L},$$

where the $-1/L$ subtracts the zero mode. The leading term $m = 0$ recovers the infinite-line heat kernel [eq:heat_kernel]; the finite-size correction is bounded by

$$\left| K_L(\ell, t) - \frac{1}{\sqrt{4\pi Dt}} e^{-\ell^2/(4Dt)} \right| \leq \frac{2}{\sqrt{4\pi Dt}} \sum_{m \geq 1} \exp\left(-\frac{(mL - \ell)^2}{4Dt}\right) + \frac{1}{L}.$$

For $\ell \leq L/2$ and $tD \leq \kappa L^2$ with $\kappa < 1/16$, the dominant correction is $O\left(e^{-(1-2\ell/L)^2/(16\kappa)}\right)$, exponentially small in $1/\kappa$. This justifies using the continuum inversion for τ_{copy} in the pre-asymptotic window $t \ll L^2/D$.

Small-System ED Illustration: Threshold and Receiver-Size Dependence

This appendix provides an *illustrative* numerical check of the smooth dependence on the operational threshold η and on the receiver size $|B|$ that is made explicit by the Gaussian-kernel inversion formula [eq:tau_lambertW]. We emphasize the intended scope: these exact-diagonalization (ED) runs are performed at a small size ($L = 8$) to keep the computation exact and fully reproducible within the submission bundle. They are included to demonstrate that (i) changing η changes the extracted copy time smoothly, and (ii) enlarging the receiver region increases the advantage and therefore reduces the inferred copy time, as expected in transport-limited regimes. They do *not* establish thermodynamic-limit scaling.

 doi:10.20944/preprints202601.0364.v3

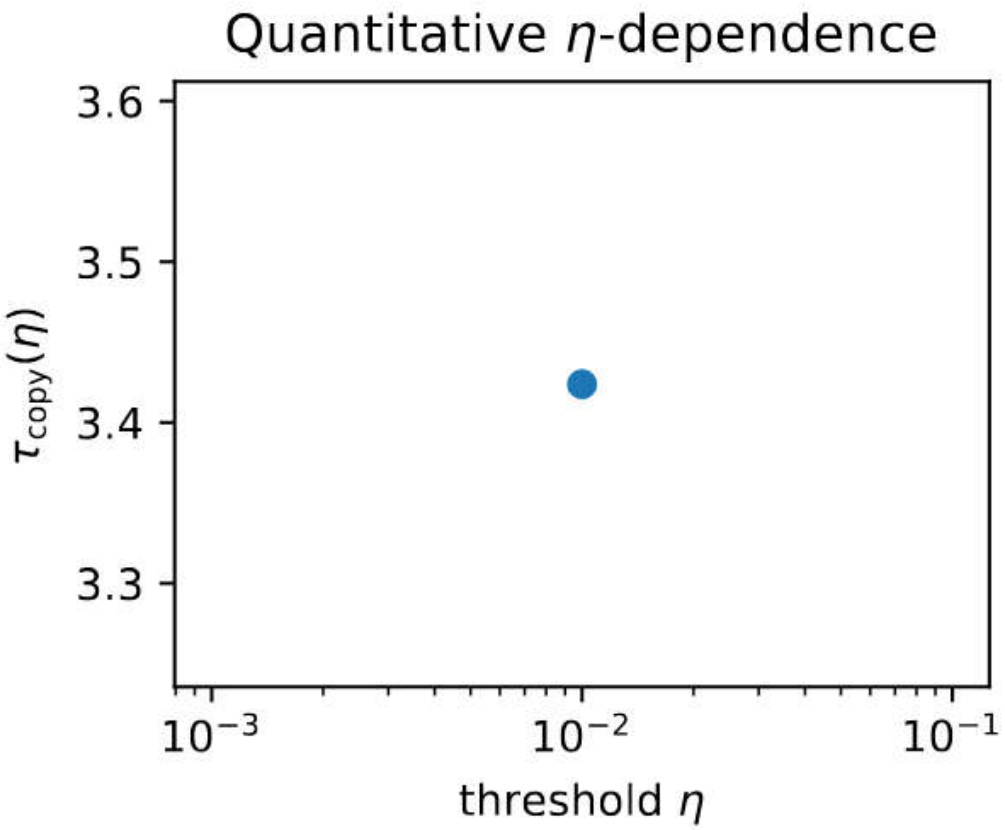

Table 8. *as the operational threshold η is varied, for a fixed sender–receiver separation in the same model and hypothesis class as Figure 2. The dependence on η is smooth on the accessible window, consistent with the slowly varying (Lambert-W/logarithmic) threshold factor in Eq. [eq:tau_lambertW].*

 doi:10.20944/preprints202601.0364.v3

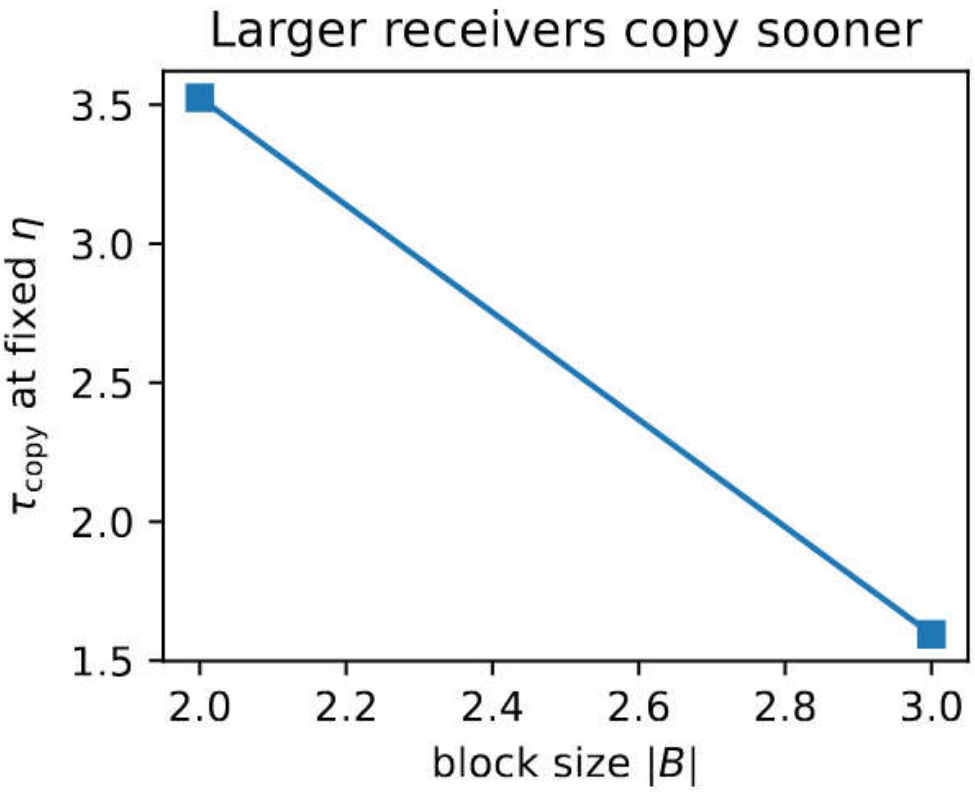

Receiver-size dependence (ED, small system). *Advantage and inferred copy-time trend as the receiver block size* $|B|$ *is increased (same ED run family). Enlarging* B *increases the receiver prefactor* K_B *in Eq. [eq:threshold_kernel_form], leading to earlier threshold crossing, consistent with Eq. [eq:tau_lambertW].*

Gaussian Discrimination and Moment Sufficiency: An Explicit Bound

Assume that, in the hydrodynamic window, the receiver's relevant fluctuation variable X_B (e.g., coarse-grained charge in B) is approximately Gaussian under both hypotheses, with means $\pm m(t)$ and common variance $\sigma^2(t)$. Then the optimal Helstrom measurement reduces (in the classical limit) to thresholding X_B, and the resulting advantage is

$$\mathrm{Adv}^{\mathrm{full}}(t) \approx \mathrm{TV}\left(\mathcal{N}\left(m(t),\sigma^2(t)\right),\mathcal{N}\left(-m(t),\sigma^2(t)\right)\right) = \mathrm{erf}\left(\frac{m(t)}{\sqrt{2}\sigma(t)}\right).$$

For small signal-to-noise ratio m/σ, $\mathrm{Adv}^{\mathrm{full}}(t) \sim \sqrt{\frac{2}{\pi}}\frac{m(t)}{\sigma(t)}$. Since $m(t)$ is controlled by the diffusion kernel [eq:signal_scaling] and $\sigma(t)$ is set by equilibrium fluctuations, low moments (mean and variance) are sufficient to determine the advantage at leading order. This provides a principled route to moment-channel near-optimality in regimes where the fluctuation algebra is approximately Gaussian.

Additional Numerical Tables and Metadata

Finite-size "effective-exponent" diagnostics (including negative/drifting slopes at the integrable point) are provided as CSV tables in the bundled SC1 data archive (see *FIGURE_MAP.md*); in the main PDF we treat these quantities strictly as *breakdown diagnostics* rather than physical exponents.

 doi:10.20944/preprints202601.0364.v3

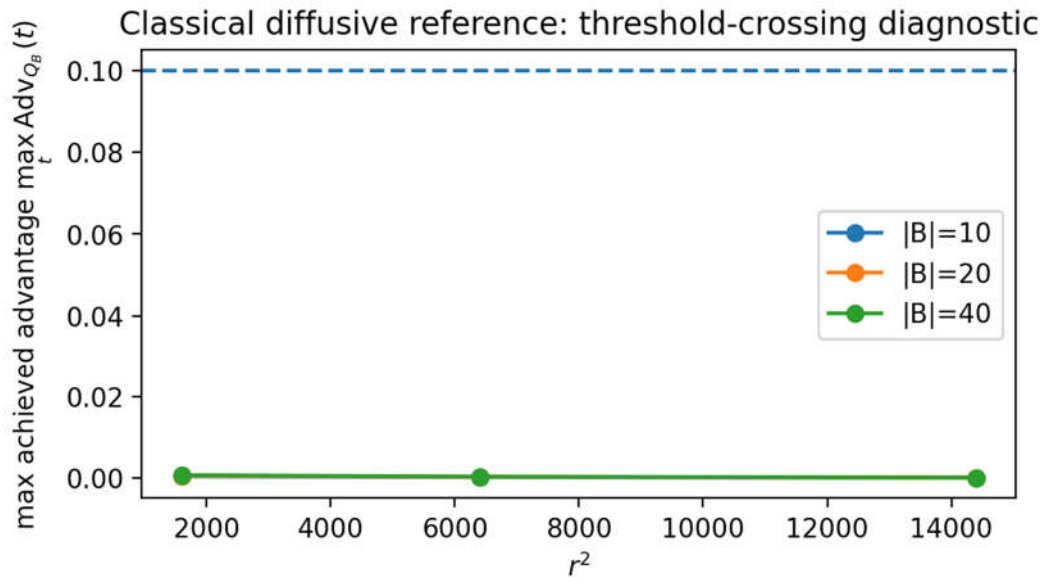

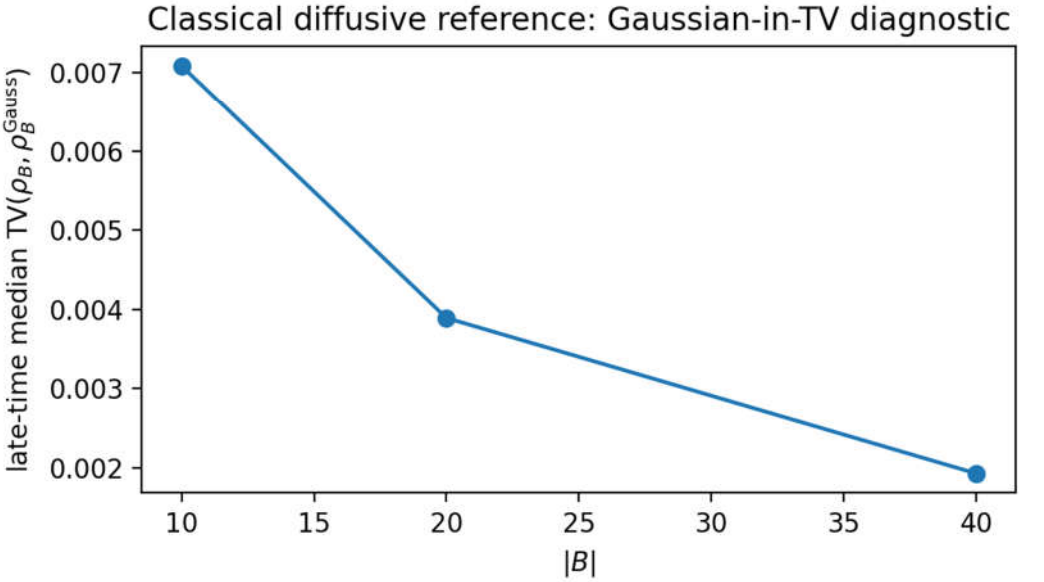

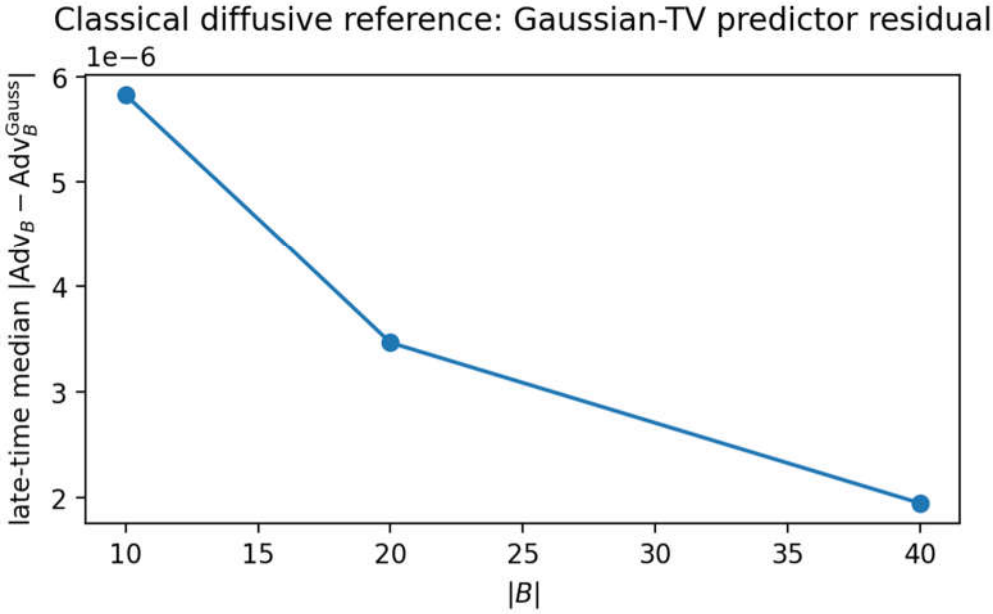

 doi:10.20944/preprints202601.0364.v3

Selected pipeline diagnostics (Appendix). Top: a threshold-crossing diagnostic for the classical diffusive reference at $\eta = 0.1$ *(dashed line), showing that for this conservative parameter set the receiver advantage stays below threshold, hence* $\tau_{copy} = \infty$ *(no crossing) while* $max_t\, Adv^{full}$ *remains small. Middle: Gaussian approximation error (trace-distance proxy) versus receiver size. Bottom: predictor residual versus receiver size for a regression-based proxy. The full diagnostic set (including parameter sweeps) is included in the SC1 data archive (Appendix 21).*

Additional numerical diagnostics and reporting details (including window scans and stability checks) used to assess the single-mode window at the accessible sizes are included in the SC1 data archive (see *FIGURE_MAP.md*). Supplementary S2 is reserved for the TEBD/MPS protocol outline. We recommend interpreting small-L "effective exponents" only as diagnostics of hydrodynamic breakdown, not as physical exponents in integrable regimes.

Reproducibility: Run Manifest and Code Pointers

For reproducibility, Supplementary Files S1–S4 and the Supplementary Code Archive SC1 include:

- definitions, locality bounds, and technical lemmas supporting the operational setup (Supplementary File S1);
- a detailed TEBD/MPS protocol and convergence checklist for future thermodynamic-limit copy-time tests (protocol only; Supplementary File S2);
- the rigorous Q-SSEP benchmark and supporting derivations for the diffusive lower bound (Supplementary File S3);
- conceptual positioning relative to OTOCs and toy examples separating receiver-limited certifiability from operator-growth diagnostics (Supplementary File S4);
- the code, parameter registries, integrity checks, fit-window scans, and the minimal data bundle used to generate the reported ED diagnostics and Helstrom-advantage figure suite (Supplementary Code Archive SC1 together with the accompanying data archive).

Reproducibility Pointers (ED Extraction and Post-Processing)

To avoid over-promising numerics that are not explicitly reported, we separate *protocol descriptions* from *computed results*. All ED-based figures and tables reported in this work can be reproduced from the bundled Supplementary Code Archive SC1 together with the accompanying analysis data archive. A concise map from each manuscript figure/table to the corresponding script, command line, and output file is provided in *FIGURE_MAP.md* (included in the accompanying Supplementary Materials and Code Archive). For the operational numerics in Section 10.2, the figure-generation scripts and the corresponding raw outputs are indexed in extttFIGURE_MAP.md within the accompanying code archive.

TEBD/MPS Protocol (Not Used for the Results Reported Here)

Supplementary File S2 provides a detailed, implementation-agnostic TEBD/MPS protocol and convergence checklist intended for future thermodynamic-limit tests of copy-time scaling. We do *not* report TEBD/MPS simulation results here, and no main-text claim relies on TEBD. Accordingly, SC1 does not include TEBD source code (which would depend on a specific tensor-network library such as TeNPy or ITensor); instead, S2 is written so that an independent group can implement the protocol in their preferred framework.

Supplementary Materials: The following supporting information can be downloaded at the website of this paper posted on Preprints.org, Supplementary File S1: definitions, locality bounds, and technical lemmas supporting the operational setup. Supplementary File S2: TEBD/MPS protocol and convergence checklist for thermodynamic-limit copy-time tests (protocol only; no TEBD results reported). Supplementary File S3: rigorous Q-SSEP benchmark and additional derivations for the diffusive lower bound. Supplementary File S4: conceptual

 doi:10.20944/preprints202601.0364.v3

positioning relative to OTOCs and toy examples separating operator growth from receiver-limited certifiability. Supplementary File S5: strengthened appendix turning the conceptual framework into (i) a diagnosis-changing phenomenon, (ii) minimal-assumption theorem statements, (iii) an experimental readout protocol with shot/readout-noise accounting, and (iv) large-scale anomalous-transport scaling templates. Supplementary Code Archive SC1: code, minimal data, and scripts to reproduce the ED diagnostics and the Helstrom-advantage figure suite reported in the manuscript. Reproducibility notes: a figure-to-script map (*FIGURE_MAP.md*) is included in the code archive.

Data and Code Availability: All materials needed to reproduce the reported exact-diagonalization diagnostics and the Helstrom-advantage figure suite are included in the accompanying Supplementary Materials and Code Archive: (i) Supplementary Files S1–S5 (theory, strengthened diagnostics, and protocol descriptions) and (ii) Supplementary Code Archive SC1, including the corresponding analysis outputs and scripts needed to reproduce the reported ED diagnostics. A figure-to-script map (extttFIGURE_MAP.md) is included in the code archive. No additional microscopic TEBD/MPS results beyond ED are reported in this work; Supplementary S2 provides an implementation-agnostic protocol for future thermodynamic-limit checks, while Supplementary S5 adds large-separation hydrodynamic scaling templates and an experiment-ready receiver protocol.

Conflicts of Interest: The author declares no competing interests.

References

1. C. W. Helstrom, *Quantum detection and estimation theory*. Academic Press, 1976.
2. A. S. Holevo, "Statistical decision theory for quantum systems," *Journal of Multivariate Analysis*, vol. 3, no. 4, pp. 337–394, 1973, doi: 10.1016/0047-259X(73)90028-6.
3. R. Kubo, "Statistical-mechanical theory of irreversible processes. I. General theory and simple applications to magnetic and conduction problems," *Journal of the Physical Society of Japan*, vol. 12, no. 6, pp. 570–586, 1957, doi: 10.1143/JPSJ.12.570.
4. H. Mori, "Transport, collective motion, and brownian motion," *Progress of Theoretical Physics*, vol. 33, no. 3, pp. 423–455, 1965, doi: 10.1143/PTP.33.423.
5. R. Zwanzig, "Memory effects in irreversible thermodynamics," *Physical Review*, vol. 124, pp. 983–992, 1961, doi: 10.1103/PhysRev.124.983.
6. D. Forster, *Hydrodynamic fluctuations, broken symmetry, and correlation functions*. Benjamin, 1975.
7. A. Nahum, C. W. von Keyserlingk, T. Rakovszky, F. Pollmann, and S. L. Sondhi, "Operator hydrodynamics, OTOCs, and entanglement growth in systems with conservation laws," *Physical Review X*, vol. 8, p. 021014, 2018, doi: 10.1103/PhysRevX.8.021014.
8. V. Khemani, A. Vishwanath, and D. A. Huse, "Operator spreading and the emergence of dissipative hydrodynamics under unitary dynamics with conservation laws," *Physical Review X*, vol. 8, p. 031057, 2018, doi: 10.1103/PhysRevX.8.031057.
9. D. Bernard and T. Jin, "Anomalous scaling and diffusion in the quantum symmetric simple exclusion process," *Communications in Mathematical Physics*, vol. 383, pp. 659–712, 2021, doi: 10.1007/s00220-021-04066-3.
10. A. Nahum, S. Vijay, and J. Haah, "Operator spreading in random unitary circuits," *Physical Review X*, vol. 8, p. 021014, 2018, doi: 10.1103/PhysRevX.8.021014.
11. C. W. von Keyserlingk, T. Rakovszky, F. Pollmann, and S. L. Sondhi, "Operator hydrodynamics, OTOCs, and entanglement growth in systems without conservation laws," *Physical Review X*, vol. 8, p. 021013, 2018, doi: 10.1103/PhysRevX.8.021013.
12. S. Xu and B. Swingle, "Scrambling dynamics and out-of-time-ordered correlators in quantum many-body systems," *PRX Quantum*, vol. 5, p. 010201, 2024, doi: 10.1103/PRXQuantum.5.010201.
13. V. Khemani, A. Vishwanath, and D. A. Huse, "Operator spreading and the emergence of dissipative hydrodynamics under unitary evolution with conservation laws," *Physical Review X*, vol. 8, p. 031057, 2018, doi: 10.1103/PhysRevX.8.031057.

 doi:10.20944/preprints202601.0364.v3

14. T. Rakovszky, F. Pollmann, and C. W. von Keyserlingk, "Diffusive hydrodynamics of out-of-time-ordered correlators with charge conservation," *Physical Review X*, vol. 8, p. 031058, 2018, doi: 10.1103/PhysRevX.8.031058.
15. B. Schumacher and R. F. Werner, "Reversible quantum cellular automata." arXiv:quant-ph/0405174, 2004.
16. D. Gross, V. Nesme, H. Vogts, and R. F. Werner, "Index theory of one dimensional quantum walks and quantum cellular automata," *Communications in Mathematical Physics*, vol. 310, pp. 419–454, 2012, doi: 10.1007/s00220-011-1353-3.
17. P. Arrighi, V. Nesme, and R. Werner, "Unitarity plus causality implies localizability," *Journal of Computer and System Sciences*, vol. 101, pp. 26–40, 2019, doi: 10.1016/j.jcss.2018.08.004.